applied sciences

MDPI

Article

Corrosion Fatigue Assessment of Bridge Cables Based on Equivalent Initial Flaw Size Model

Zhongxiang Liu [1], Tong Guo [2,*], Xiaming Yu [3], Shilei Niu [1] and José Correia [4]

[1] School of Transportation, Southeast University, Nanjing 210096, China; zhongxiang@seu.edu.cn (Z.L.); niushilei123@outlook.com (S.N.)
[2] Key Laboratory of Concrete and Prestressed Concrete Structures, Ministry of Education, Southeast University, Nanjing 210096, China
[3] School of Civil Engineering, Southeast University, Nanjing 210096, China; yxm1666@outlook.com
[4] CONSTRUCT & Faculty of Engineering, University of Porto, 4099-002 Porto, Portugal; jacorreia@fe.up.pt
* Correspondence: guotong@seu.edu.cn

Abstract: Bridge cables under traffic loads are more prone to failure during the service life due to the corrosion–fatigue coupling effect. In this study, a novel lifespan model based on the equivalent initial flaw size (EIFS) theory is established to analyze the various stages of the lifespan of steel wires. Additionally, a comprehensive corrosion-fatigue lifespan calculation method for parallel steel wire cable is established based on the series–parallel model. A case study of the Runyang Suspension Bridge is conducted to evaluate the evolution of corrosion-fatigue damage in bridge cables during the service life. The results indicate that under the action of corrosion-fatigue, steel wires are more prone to crack initiation, and their fracture toughness is further reduced. In cases where the corrosion level is relatively low, the steel wires of the bridge cables experience no corrosion-fatigue fracture. When the steel wires have initial defects and are subject to corrosion-fatigue conditions, their fracture lifespan is dependent on the severity of the corrosive medium. The reduction in the service life of the cables under the corrosion environment is much greater than that under heavy loads. This research may contribute to the understanding of corrosion-fatigue damage in bridge cables, involving assessment, maintenance, and replacement for bridge cables.

Keywords: bridge cables; EIFS; corrosion fatigue; crack initiation; lifespan assessment

check for updates

Citation: Liu, Z.; Guo, T.; Yu, X.; Niu, S.; Correia, J. Corrosion Fatigue Assessment of Bridge Cables Based on Equivalent Initial Flaw Size Model. *Appl. Sci.* **2023**, *13*, 10212. https://doi.org/10.3390/app131810212

Academic Editor: Giuseppe Lacidogna

Received: 18 August 2023
Revised: 7 September 2023
Accepted: 9 September 2023
Published: 11 September 2023

Copyright: © 2023 by the authors. Licensee MDPI, Basel, Switzerland. This article is an open access article distributed under the terms and conditions of the Creative Commons Attribution (CC BY) license (https://creativecommons.org/licenses/by/4.0/).

1. Introduction

As the primary load-bearing component of bridges, cable systems have a significant impact on its safety and usability [1,2]. During the service life, the cable components experience high-stress conditions and frequent stress variations while undergoing environmental corrosion [3–5]. The effect of corrosion is particularly relevant for cable-supported bridges located in harsh marine environments [6]. Corrosion fatigue is a degradation form of metallic materials resulting from the combined effect of corrosion and fatigue. The effect of corrosion fatigue is more severe than the sum of individual corrosion and fatigue damages, which is closely related to the electrochemical corrosion of metals [7–9]. Extensive studies have been conducted on the development mechanisms, quantitative methods, and influencing factors of corrosion fatigue [10–12]. The existing research generally divides the process of corrosion fatigue damage development into the pitting corrosion stage and the corrosion fatigue cracking stage [13,14].

During the development stage of pitting corrosion, the depth and shape of the pits are primarily controlled by corrosion [15]. Godard [16] observed the evolution of pit depths in metallic plates submerged in water and derived an equation describing the evolution of pit depths under corrosion fatigue. The results indicated that the pits would gradually expand into semi-circular shapes under corrosion fatigue. Hosni et al. [17] studied the influence of different types of intermetallic compound particles on pitting

corrosion and its morphology development in seawater for aluminum alloys through electrochemical corrosion tests. When the pitting corrosion reaches a certain stage, the bottom of the pit meets the critical conditions for crack extension, and the corrosion fatigue process enters the crack growth stage dominated by fatigue [18]. This critical condition is known as pit nucleation. Kim et al. [19] considered the accumulating effect of local plastic deformation of pits under cyclic loading and further improved the crack nucleation model. During the crack propagation stage dominated by fatigue stresses, the corrosion accelerates crack propagation, making the crack propagation process highly complex [20]. Gangloff et al. [21] conducted corrosion fatigue tests on steel and concluded that load factors, geometric characteristics, and environmental factors play dominant roles in corrosion fatigue. Olive et al. [22] studied the hydrogen ion migration during the crack propagation of steel wires in magnesium chloride solution through corrosion fatigue tests, while Shipilov [23] believed that the crack propagation rate in a corrosive fatigue environment is related to the hydrogen ions released during crack tip extension. Based on the concept of a fracture process zone, crack propagation rate models have been established and validated. Currently, there is no universally accepted and comprehensive analysis method for the development of pitting corrosion during corrosion fatigue, despite the existing research progress.

Corrosion leads to the formation of pits and weakens the cross-sectional area, thereby increasing the average stress level and local stress concentration on the bridge cables. Under the combined action of corrosion and stress range variation, local pits gradually develop into crack nucleation and eventually propagate until failure. Martin et al. [24] analyzed the crack propagation rate of the bridge wire in artificial seawater and found that the crack propagation rate of microcracks was significantly higher than that of long cracks with the behavior of long crack propagation following the Paris equation. Li et al. [25] conducted mechanical tests and fatigue loading on service-exposed cables and found that the ultimate strength of the wire was minimally affected by corrosion, but the ductility of the corroded wire significantly decreased. Liu et al. [26] conducted acidic salt spray tests and immersed corroded wires in sodium chloride solutions for fatigue loading, showing a significant reduction in the fatigue lifespan of corroded wires.

The concept of equivalent initial flaw size (EIFS) was established to evaluate the crack initiation lifespan [27]. It is defined as the predicted long crack propagation model starting from EIFS, which is consistent with actual fatigue crack propagation [28]. The following two aspects should be noted: (1) EIFS is not a physical quantity associated with the component; (2) EIFS is a hypothetical flaw size that can be used as the initial crack size in the long crack propagation model [29].

Based on the EIFS theory, this study presents a novel lifespan model to quantitatively analyze the various stages of lifespan and the impact of corrosion and corrosion–fatigue coupling for steel wires. In Section 2, “Corrosion Fatigue Lifespan Model based on EIFS Theory”, the EIFS theory is expounded and the corrosion fatigue lifespan model of the steel wire based on the EIFS theory has derived and illustrated. In Section 3, “Corrosion Fatigue Performance of Steel Wire”, fatigue lifespan evaluation of the steel wire and quantitative analysis of corrosion fatigue coupling effect are conducted. In Section 4, “Corrosion Fatigue Lifespan Assessment of Parallel Wire Cable”, a comprehensive corrosion-fatigue lifespan calculation method for parallel steel wire cables is established based on the series–parallel fiber bundle model, and a case study of Runyang Suspension Bridge is conducted. The novelties of the approach are as follows: the life model based on the EIFS can consider the various stages (short crack propagation and long crack propagation) of lifespan and quantitatively analyze the impact of corrosion and corrosion–fatigue coupling for steel wires. This research may contribute to the study of corrosion-fatigue damage in bridge cables, involving assessment, maintenance, and replacement for the bridge cables.

2. Corrosion Fatigue Lifespan Model Based on EIFS Theory

2.1. EIFS Theory

The key of fatigue lifespan prediction lies in determining the crack initiation point. In the case of small-sized specimens, the crack propagation lifespan is usually considered negligible compared to the overall fatigue lifespan. Thus, the entire fatigue lifespan is nearly equal to the crack initiation lifespan. However, the crack initiation lifespan is only a part of the overall lifespan for large-sized structures. In this scenario, the crack initiation lifespan is closely related to the critical size of crack nucleation. At present, there are three main methods for determining the critical size. One method is to empirically define a crack size as the critical size, which is usually between 0.25 and 1 mm for metals [30]. Another method is to use non-destructive testing to detect the crack nucleation size [31]. However, current non-destructive testing methods are unable to truly detect the size of the crack nucleation. If the empirically defined or non-destructive testing crack nucleation size is used, the predicted results tend to be overly optimistic. Therefore, the EIFS theory is introduced as a third method for determining the critical size of crack nucleation, which has been proven to be a practical method for evaluating crack initiation and fatigue lifespan [32].

The method of EIFS was initially proposed to address the issues in fracture mechanics-based fatigue lifespan prediction models. It is well known that the surface of any specimen is never perfectly smooth and always contains various types of defects, including intentional defects and corrosion defects as well as accidental scratches and impact-induced defects. All these surface defects can be equivalently treated as hypothesized cracks with known initial sizes, which are referred to as EIFS. The next question is how to determine EIFS. Surface-nucleated cracks generally exhibit typical short crack characteristics. It is well known that the crack growth behavior of short cracks is significantly different from that of long cracks [33–35]. Figure 1 illustrates the crack growth behavior of short cracks and long cracks in the near-threshold region, where a, N, and da/dN are the crack length, loading cycle number and the crack growth rate. In addition, ΔK, ΔK_{th} and K_p represent the stress intensity factor range, threshold value of the material for crack initiation and critical stress intensity factor.

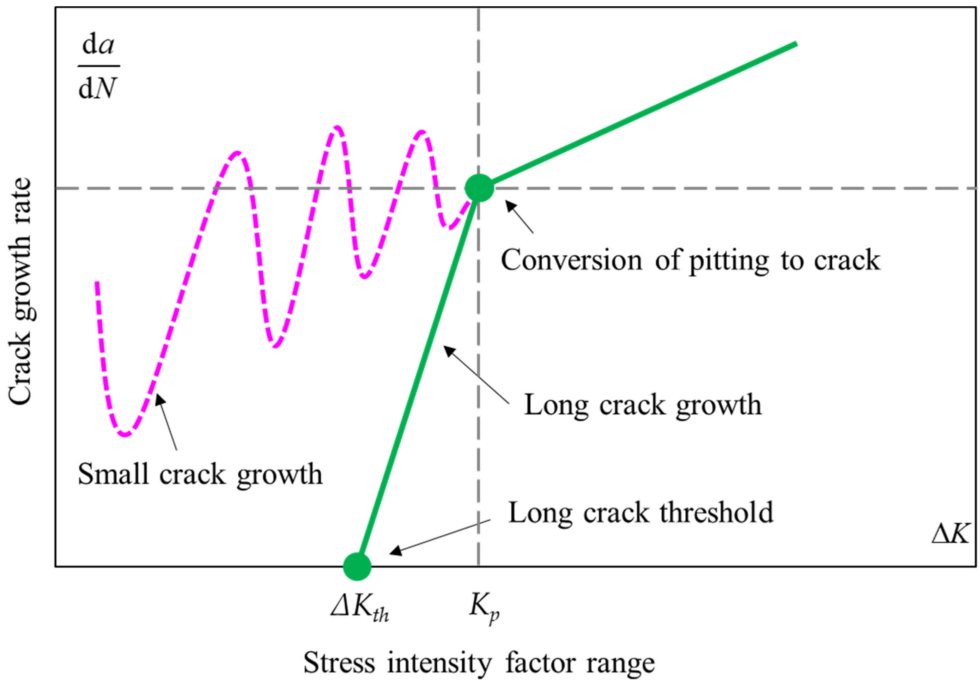


Figure 1. Schematic diagram of crack propagation.

It can be observed that in the near-threshold region, the fluctuating small crack growth curve deviates significantly from the long crack growth curve. When the stress intensity

factor reaches the critical stress intensity factor, small cracks will develop toward long cracks under the influence of a pitting pit. Hence, the usage of a long crack growth threshold to calculate EIFS is unreasonable. Since it is challenging to measure the crack growth curve of small cracks, the EIFS theory employs the extension of the linear portion of the Paris law as a surrogate for the short crack growth curve. Typically, the crack extension threshold for short cracks is taken as the Paris equation's slope extended to 10^{-10} mm/cycle of the stress intensity factor range. The feasibility of this approach has been demonstrated in the literature [36].

Based on the EIFS theory [27], the initiation lifespan of corrosion fatigue cracks, also known as pitting, is considered as part of crack propagation, as shown in Figure 2. Once the initial equivalent defect is determined, the crack initiation lifespan of the corroded steel wire is equivalent to the integration from this equivalent initial crack depth to the critical crack depth under the long crack extension law. As the crack size decreases, the propagation rate of a long crack approaches an asymptotic trend, which is known as the crack threshold. Small cracks with the same stress intensity factor range propagate at a rate several times faster than what is predicted by the data for long crack propagation. However, the mechanism of small crack growth is not yet fully understood, and the propagation of small cracks largely depends on the material's microstructural features, including grain size, grain orientation, and initial defect shape. These structural factors exhibit significant uncertainty due to their stochastic nature. This introduces additional challenges for probabilistic life prediction. To overcome these difficulties, the EIFS concept avoids the analysis of small crack growth and instead utilizes an equivalent initial crack size that matches the fatigue life of the specimen during the analysis of long crack growth. The detailed calculation process will be discussed in Section 2.2.

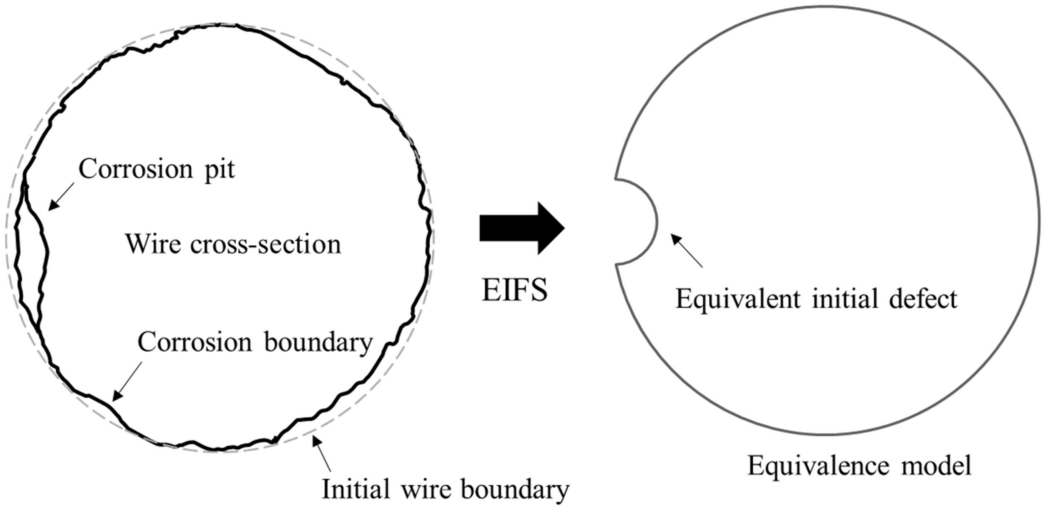


Figure 2. EIFS schematic of corroded wire cross-section.

2.2. Corrosion Fatigue Lifespan of Steel Wire

The crack nucleation lifespan (N_n) can be calculated by Equation (1) [32]:

$$N_{\mathrm{n}} = \frac{9\Delta K_{th}^2 G}{2E(\sigma - \sigma_f)^2 a_0} \tag{1}$$

where G represents the shear modulus and E represents the elastic modulus, with a relationship of $G = E/(2(1 + v))$, where v is the Poisson's ratio and is taken as 0.3. When considering the local stress concentration effect of the corrosion pit, as the corrosion test does not alter the material's elastic region constitutive relationship, from the perspective of linear elastic fracture mechanics, the threshold value of the material ΔK_{th} for crack initiation does not change with the fatigue limit σ_f. For high-strength steel wire, the fatigue limit σ_f is taken as

247.5 MPa [37]. Since the fatigue initiation often occurs at the bottom of the corrosion pit, the effect of stress concentration should be considered when calculating the stress σ in the above equation. It can be calculated using the following equation:

$$\sigma = K_t \cdot \sigma_s \tag{2}$$

$$\sigma_s = \Delta F_a / S_{corr} \tag{3}$$

$$K_t = \frac{1 + 6.6 \cdot a_p / c_p}{1 + 2 \cdot a_p / c_p} \tag{4}$$

where K_t is the stress concentration coefficient, ΔF_a is the load value of the pulsatile stress amplitude, σ_s is the stress of the corroded steel wire, S_{coor} is the cross-section area of the corroded steel wire, and a_p and c_p are the depth and width of the pit.

Due to the large number of small cracks and no obvious propagation law, it is difficult to quantify the evolution mode. In some studies in the literature [38,39], an equivalent empirical model based on the Paris formula is given considering the calculation method of fatigue lifespan:

$$N_{sc} = \frac{a_0^{(1-m_{sc}/2)} - a_{sc}^{(1-m_{sc}/2)}}{C_{sc}(2\sigma_s)^{m_{sc}} \beta^{m_{sc}} \pi^{m_{sc}/2} (\frac{m_{sc}}{2} - 1)} \tag{5}$$

where β is the shape parameter of small crack propagation, and the value is taken as $0.5\sqrt{\eta}$ [40]. C_{sc} and m_{sc} are material constants for short crack propagation, which are 9×10^{-11} and 3.3, respectively [41]. When the initial defect depth a_0 reaches the critical depth of small crack a_{sc}, the small crack will be transformed into a long crack. a_{sc} refers to the crack depth when the crack depth reaches the threshold value of the stress intensity factor, which is calculated by Equation (6):

$$a_{sc} = \frac{\Delta K_{th}^2}{\pi Y^2 (2\sigma_s)^2} \tag{6}$$

The solution of the form factor formula for the arc crack Y is given by Forman et al. [42]:

$$Y(\frac{a}{D}) = 0.92 \cdot \frac{2}{\pi} \cdot \sqrt{\frac{2D}{\pi a} \tan \frac{\pi a}{2D}} \cdot \frac{0.752 + 1.286(\frac{a}{D}) + 0.37(1 - \frac{\pi a}{2D})^3}{\cos \frac{\pi a}{2D}} \tag{7}$$

where a is the crack size and D is the wire diameter.

The fatigue long crack growth lifespan N_{lc} is calculated by the Paris formula:

$$N_{lc} = \int_{a_{sc}}^{a_c} \frac{1}{C_{lc}(\Delta K)^{m_{lc}}} da \tag{8}$$

$$\Delta K = K_{\max} - K_{\min} = Y(2\sigma_s)\sqrt{\pi a} \tag{9}$$

where C_{lc} and m_{lc} are the material constants of long crack propagation, which are 6×10^{-11} and 3.3, respectively [41]. The critical crack depth a_c is calculated using the observed fracture value. ΔK is the equivalent stress intensity factor at the pit bottom.

The fatigue lifespan N_F of corroded steel wire is shown as follows:

$$N_F = N_n + N_{sc} + N_{lc} \tag{10}$$

The procedure for calculating the EIFS of corroded steel wires is illustrated in Figure 3. The detailed calculation steps are listed below:

(1) The fracture morphology characteristics of steel wire were obtained through a corrosion fatigue test, e.g., depth of erosion pit a_p, width of erosion pit c_p, area of fracture

S_{coor}, depth of main crack a_c, and depth of facture D_{coor}. The number of fatigue sources is also recorded.

(2) According to the number of fatigue sources, the type of fatigue source expansion is determined, and the initial crack value a_0 is tentatively determined.

(3) The fatigue life N_F of corroded steel wire is calculated by substituting the parameter values obtained in steps (1) to (2) into Equations (1)–(10).

(4) Determine whether the relative error between the calculated fatigue life (N_F) of the corroded steel wire and the actual fatigue life (N_E) is less than 1%. If it is, the value of a_0 obtained from step (2) is the EIFS. If not, increase the value of a_0 by 1×10^{-6} and use it as the corrected a_0 value; then, repeat the evaluation process of step (4).

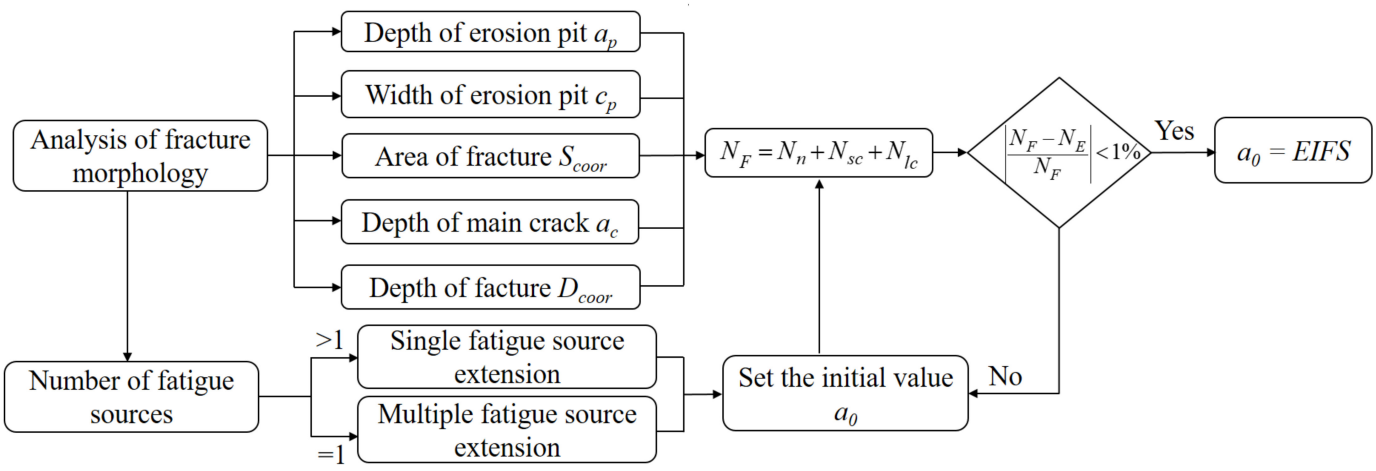


Figure 3. Calculation procedure of EIFS.

3. Corrosion Fatigue Performance of Steel Wire

Corrosion fatigue coupling tests were carried out on high-tensile steel wires using an innovative corrosion fatigue test method proposed by Liu et al. [26]. The proposed lifespan model based on the EIFS theory was used to analyze the fatigue lifespan of corroded steel wires at various stages and the effect of corrosion–fatigue coupling on the lifespan.

3.1. Fatigue Lifespan Evaluation of Steel Wire

The tested steel wire used here had a length of 300 mm, a nominal tensile strength of 1670 MPa (measured average tensile strength was 1935 MPa), a sample diameter of 5.4 mm, and a diameter of 5.25–5.27 mm after removing the coating. This study used 5.26 mm for calculations. Furthermore, the two-dimensional dimensions of corrosion fatigue sample fracture pits were extracted, and the influence of these pits on fatigue life was analyzed. The two-dimensional pit dimensions mainly consisted of the pit depth (a_p) and width (c_p), which were measured as shown in Figure 4. The three-point circle method was used to process the corroded cross-section. The three blue dots in Figure 4 are on the edge of the corroded cross-section and the red dot is the center of the circle determined by blue dots. Multiple lines were drawn from the center of the circle to the inner wall boundary of the pit. The point where the shortest distance from the line intersects the pit was considered the deepest point of the pit. The lines were extended to the outer surface of the steel wire, and the extension distance represented the pit depth. Additionally, the straight-line distance between points on both sides of the two-dimensional pit was considered the pit width. The measured pit parameters are listed in Table 1.

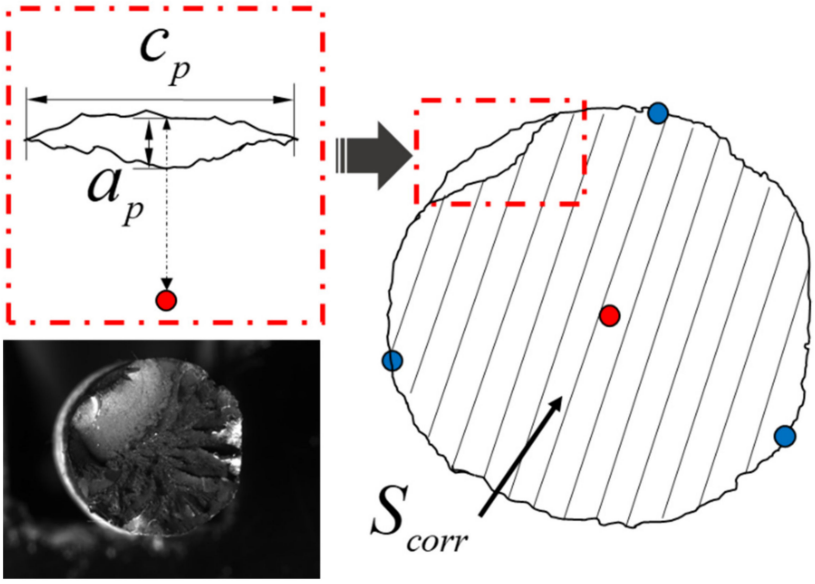


Figure 4. Pit size measurement diagram.

Table 1. Results of EIFS calculations and lifespan of each stage.

Extension Type	Depth of Erosion Pit a_p/mm	Depth of Erosion Pit c_p/mm	Fracture Area S_{coor}/mm^2	a_0 /mm	a_{sc} /mm	a_c /mm	N_n	N_{sc}	N_{lc}
single fatigue source	0.422	3.609	18.412	0.0072	0.054	2.678	635	54,526	14,818
	0.179	2.165	19.588	0.0031	0.061	2.124	8210	136,428	16,548
	0.325	2.401	18.828	0.0059	0.056	2.274	690	70,428	15,498
	0.263	2.358	19.734	0.0040	0.062	2.485	2617	114,486	16,758
	0.223	1.475	20.210	0.0043	0.065	2.453	1365	117,326	17,507
	0.124	0.629	19.135	0.0022	0.058	2.135	1001	163,434	15,894
	0.245	2.614	18.545	0.0055	0.055	2.279	1469	70,407	14,964
	0.088	0.397	19.709	0.0022	0.062	2.329	950	177,582	16,744
multi-fatigue source	0.147	1.948	18.057	0.0056	0.052	1.733	1821	63,296	14,187
	0.339	2.485	19.133	0.0068	0.058	2.205	673	66,480	15,926
	0.175	1.057	19.508	0.0051	0.061	2.198	691	90,730	16,349
	0.248	2.292	19.468	0.0068	0.060	2.556	1427	70,725	16,470
	0.278	3.307	17.948	0.0069	0.051	1.982	1076	51351	14,143
	0.126	2.579	18.419	0.0044	0.054	1.898	12,145	82,241	14,765
	0.290	1.915	17.299	0.0060	0.048	2.489	300	50,741	13,103
	0.339	2.886	16.960	0.0074	0.046	2.075	328	39,036	12,663
	0.183	2.218	18.693	0.0056	0.056	2.008	2227	71,985	15,108
	0.359	1.823	19.844	0.0073	0.063	2.146	379	71,414	16,908

The measured pit parameters are substituted into Equations (1)–(10) in Section 2.2, and the calculation conditions and procedures of the EIFS and lifespan of each stage can conducted according to Figure 3. If the fatigue lifespan N_F of the corroded steel wire is equal to the test value N_E, the initial defect depth of the corroded steel wire can be calculated. The calculation results are shown in the Table 1. The corrosion has two main aspects of impact on the fatigue lifespan: (1) The depth and width of the corrosion pit, as well as the size of the fracture area, directly affect the initiation of cracks. Deeper and wider corrosion pits, as well as larger fracture areas, can lead to a shorter crack initiation lifespan. (2) The size of the fracture area resulting from corrosion affects the rate of crack propagation. A larger fracture area can lead to faster crack growth and, consequently, a shorter crack propagation lifespan. Generally, corrosion affects the fatigue lifespan by influencing both the initiation and propagation stages of crack growth.

Since the steel wire specimens have the same mass loss rate, the average corrosion depth D_{corr} can be considered constant, and the fractures of the steel wire are primarily influenced by individual large corrosion pits. Therefore, the corrosion pit depth and width can be considered as the two main factors determining the size of the fracture area. The depth-to-diameter ratio of the corrosion pits remains approximately constant across different depths. The relationship between EIFS and the variation in corrosion pit depth is illustrated in Figure 5.

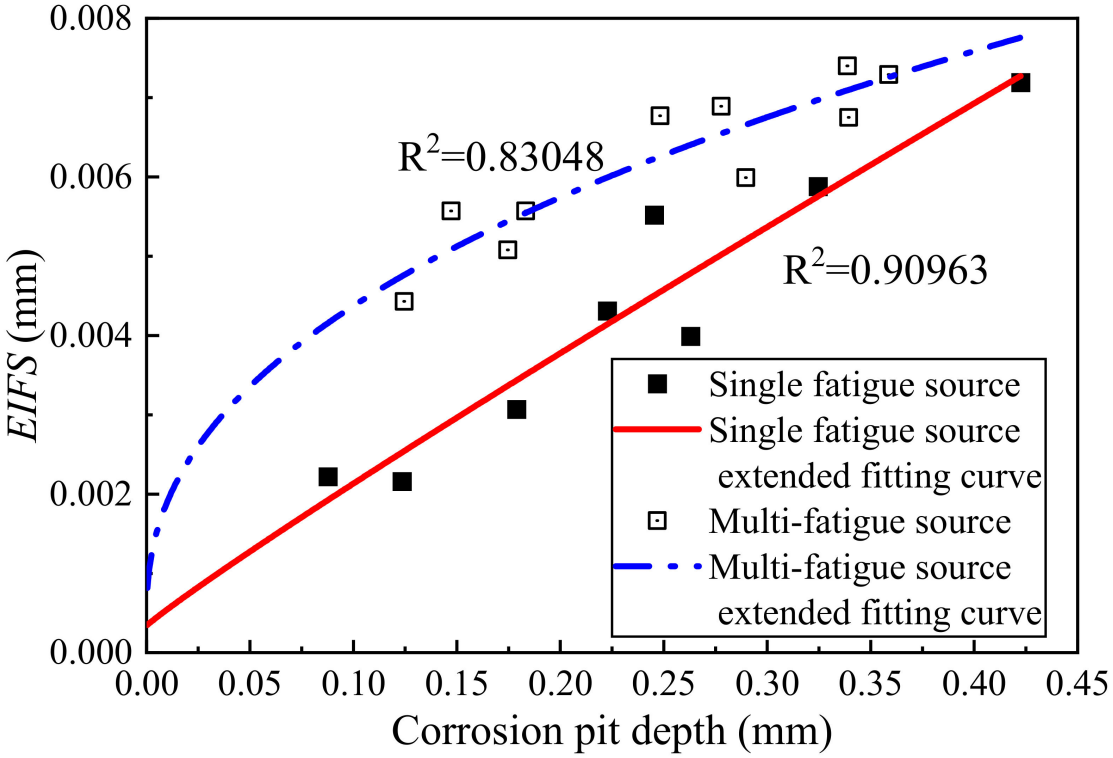


Figure 5. Relationship of EIFS with the corrosion pit depth.

The regression fitting curves for equivalent initial crack depth a_0 and corrosion pit depth for single and multiple fatigue source extension conditions are given in the following equation:

$$\begin{cases} a_0 = 0.000386 + 0.0156a_p^{0.938}, \text{for single fatigue source} \\ a_0 = 0.000443 + 0.0106a_p^{0.431}, \text{for multi fatigue source} \end{cases} \quad (11)$$

The relationship between a_0 and corrosion pit depth follows a power function, and the fitting results are satisfactory, with respective coefficients of determination of 0.90963 for single fatigue source propagation and 0.83048 for multiple fatigue source propagation. In Equation (11), when the corrosion pit depth is zero, the value of a_0 represents the equivalent initial crack depth of material micro-defects, such as polishing, scratching, and local residual stress. Under the same corrosion pit depth, the value of a_0 for multiple-source propagation is larger than that for single-source propagation, which explains that the fatigue lifespan under multiple-fatigue source propagation is smaller than that under single fatigue source propagation. As the corrosion pit depth increases, the values of a_0 for both types of propagation approach each other. Therefore, after the corrosion pit depth reaches approximately 0.4 mm, the fatigue lifespan of the two types of damaged steel wires converges.

Figure 6 depicts the variation of crack depth with fatigue lifespan for single fatigue source propagation and multiple fatigue source propagation types, considering the influ-

ence of corrosion pits. It can be observed that the EIFS values for both propagation types show minor fluctuations with different corrosion pit depths. The maximum and minimum values are within the same order of magnitude. This pattern is also reflected in the critical short crack depth a_{sc} and the critical long crack depth a_c. However, there are significant differences in the crack initiation lifespan N_n corresponding to EIFS values. For single fatigue source propagation, the minimum N_n value is 635, and the maximum is 8210, while for multiple fatigue source propagation, the minimum N_n value is 300, and the maximum is 12,145.

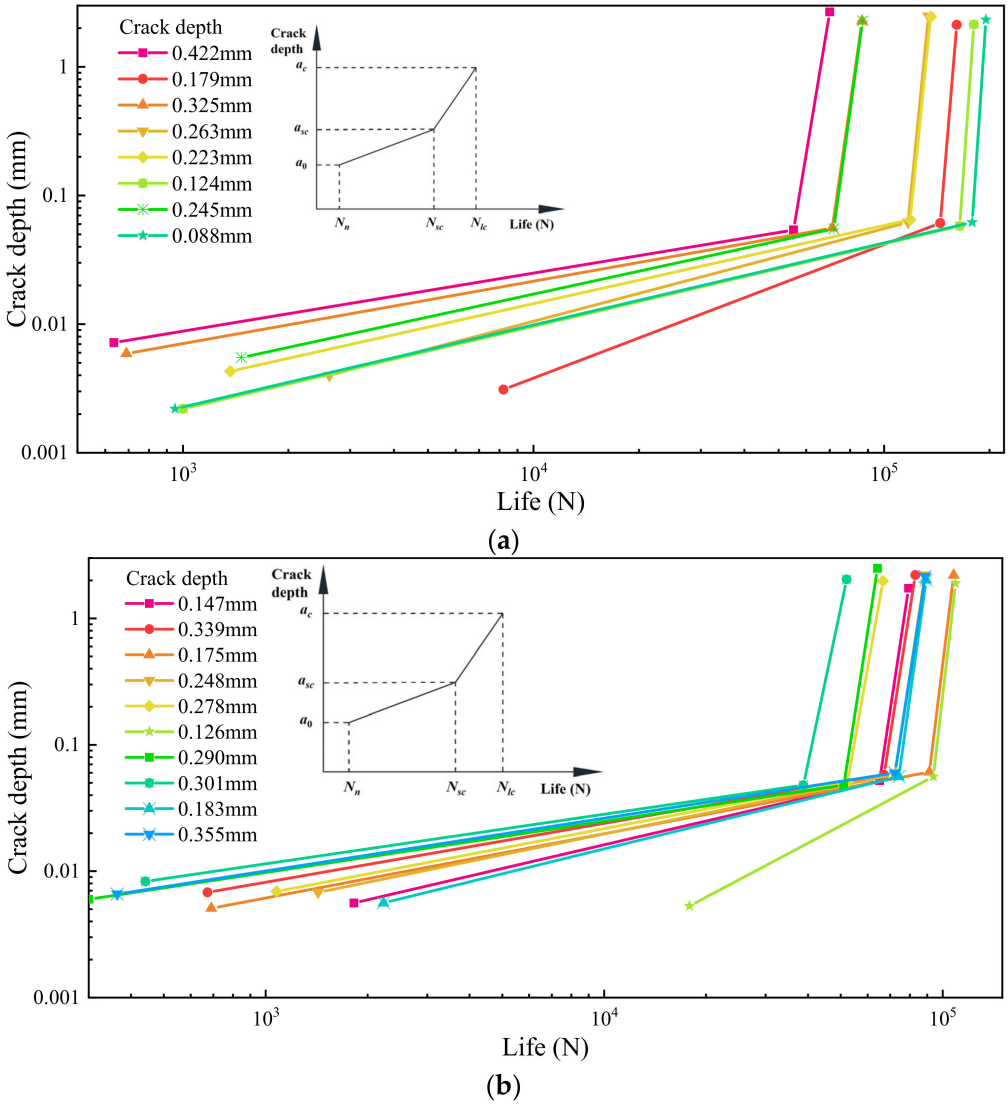


Figure 6. Relationship between crack depth and lifespan for different expansion types. (**a**) single fatigue source expansion; (**b**) multi-fatigue source expansion.

Regarding the crack initiation lifespan, as the corrosion pit depth increases, the initiation lifespan decreases for both propagation types. For the crack propagation lifespan, the lifespan is relatively similar for different corrosion pit depths. This is because factors influencing the calculation of the long crack lifespan include the crack growth threshold value ΔK_{th}, applied stress amplitude, and critical crack depth a_c, where ΔK_{th} determines the maximum depth a_{sc} of short cracks. When considering the material's linear elastic fracture mechanics behavior under the influence of corrosion surface pits, the main crack propagation plane already encompasses the two-dimensional pit surface during the propagation

of long cracks. The impact of corrosion pits is only manifested in the weakening of the cross-section, leading to increased stress amplitude.

3.2. Quantitative Analysis of Corrosion Fatigue Coupling Effect

The impact of corrosion fatigue coupling on the fatigue lifespan of the steel wire manifests in multiple stages. Before the coating fails, corrosion fatigue accelerates the electrochemical reactions of the coating. After the coating fails, the appearance of corrosion pits and the continuous action of the corrosive medium lead to an earlier initiation period of cracks and a reduction in the crack growth threshold, resulting in a decrease in the proportion of the crack initiation lifespan. The influence of corrosion fatigue on crack propagation rate is more evident with the propagation rate of long cracks increasing with the intensification of corrosion. To facilitate a comparative analysis of the impact of corrosion–fatigue coupling on fatigue lifespan, without considering the multi-stage lifespan, the corrosion pits can be simplified as single-edge cracks, and the fatigue lifespan N_F of the corroded steel wire can be calculated using Equation (12):

$$N_F = \varphi \cdot \int_{a_0}^{a_c} \frac{1}{C(\Delta K)^m} da \tag{12}$$

where the unilateral crack depth uses the EIFS value, and φ is a correction factor that takes into account the form nucleation lifespan as well as the small crack extension lifespan. In the above equation, a_0 is simplified as a parameter that is affected by the depth of the corrosion pit, while ΔK is mainly affected by the area of the corroded section. For ease of application, C and m are treated as initial crack depths in accordance with the long crack extension parameter. The above equation can be transformed into the following form:

$$N_F = \varphi(a_p) \cdot \int_{a_0(a_p)}^{ac} \frac{1}{C_{lc}(\Delta K)^{m_{lc}}} da \tag{13}$$

$$\begin{cases} \varphi(a_p) = \frac{1.08234}{a_p^{0.0764}}, \text{for single source extension type} \\ \varphi(a_p) = \frac{1.11154}{a_p^{0.04331}}, \text{for multi source extension type} \end{cases} \tag{14}$$

The detailed relationship between φ and the variation in corrosion pit depth can be seen in Figure 7. As the corrosion pit depth tends toward zero, the value of φ shows an exponential increase. This is because in the absence of corrosion pits, the stress amplitude applied to the smooth specimen (180 MPa) is lower than the fatigue limit, and its lifespan is calculated as infinite cycles. Therefore, the value of φ tends toward infinity. When the corrosion pit depth approaches the critical crack depth a_c, the value of φ gradually tends toward zero. In this case, the steel wire fractures immediately upon fatigue, resulting in a fatigue lifespan of zero. The relationship between φ and the variation in corrosion pit depth is fitted using a power function. The coefficients of determination (R^2 values) for the fitted curves of the two types of φ values are 0.85387 and 0.73303, respectively.

As shown in Figure 8, Equations (13) and (14) are used to calculate the parameters of seven fatigue specimens. The calculated fatigue lifespan values correspond well to the experimental values with an error of around 10%. Since the specimens used for corrosion fatigue in this study are from the same batch of corroded steel wire as those used by Liu et al. [26], the equation mentioned above can be used to calculate the mechanical fatigue lifespan $N_{cal,air}$ of the steel wire with the same fracture dimensions as the corroded fatigue specimens. The calculated result is shown in Figure 9, where the length of the descending straight-line segment represents the reduction in lifespan caused by the coupling effect of corrosion fatigue. This value is equal to $N_{cal,air}$ minus the corrosion fatigue test value. It can be seen that for the multi-source extended steel wire, the influence of corrosion–fatigue coupling effect on its lifespan is more pronounced.

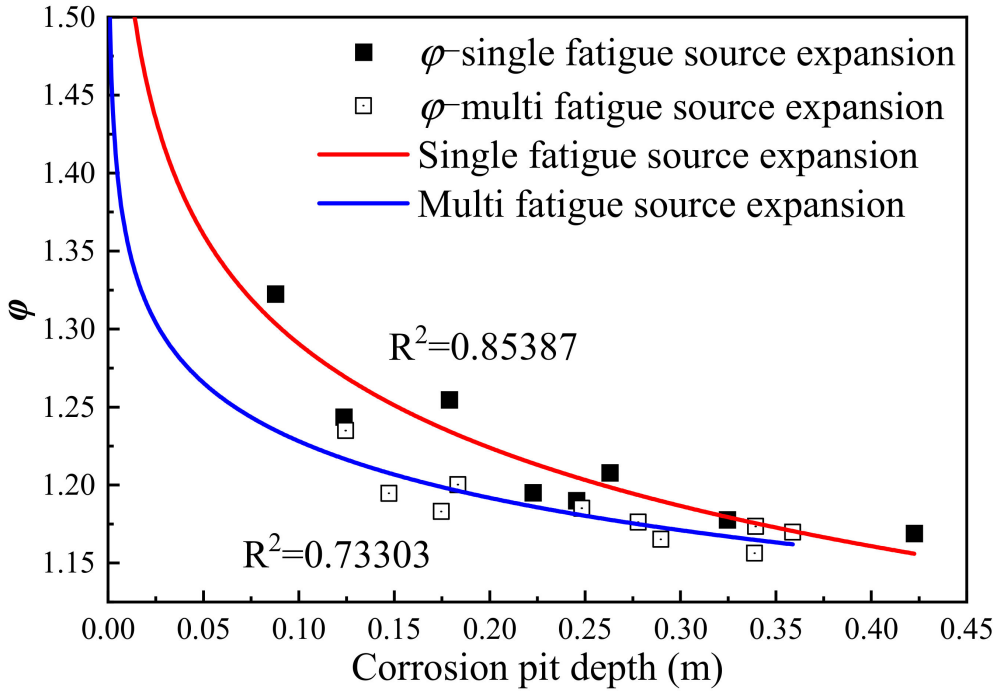


Figure 7. Relationship between φ and corrosion pit depth.

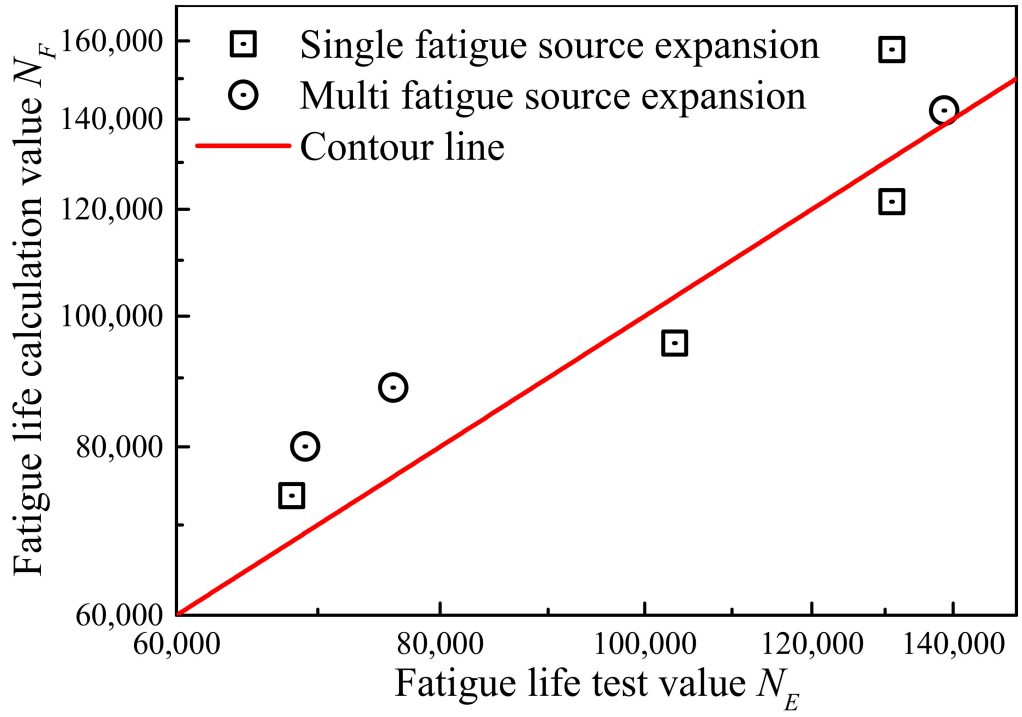


Figure 8. Comparison of model calculation results.

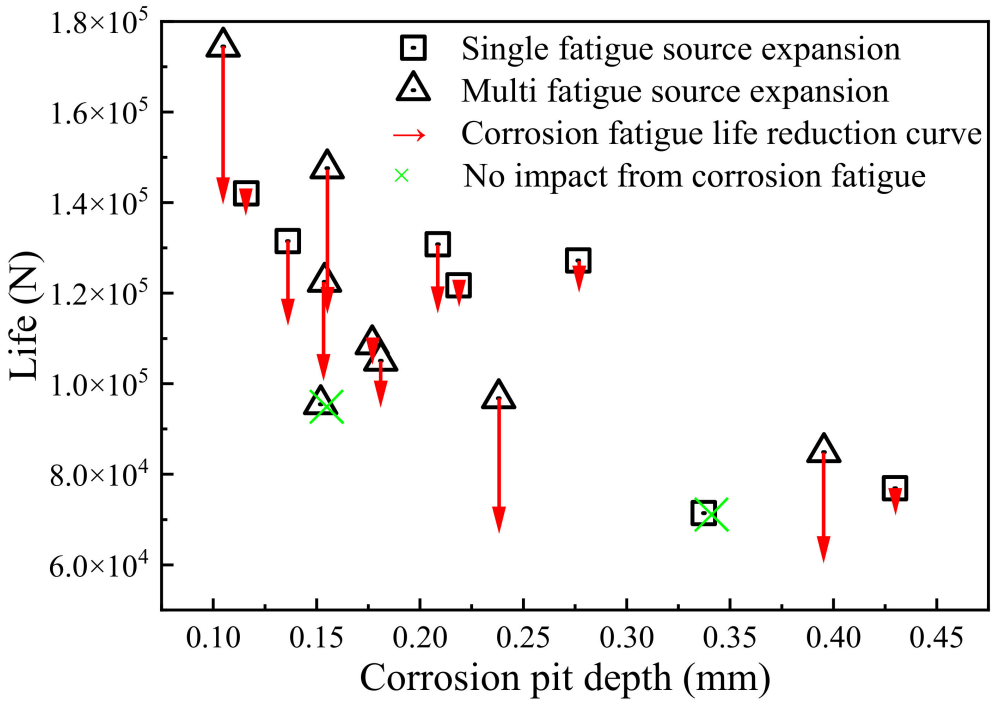


Figure 9. Lifespan reduction.

When processing the fatigue lifespan of the steel wire using Equation (12), the fatigue behavior of the wire is simplified as the integral form of the Paris equation. When considering the corrosion–fatigue coupling effect, further corrections can be made to the crack propagation rate. The modified equation is as follows:

$$N = \varphi(a_p) \cdot \int_{a_0(a_p)}^{a_c} \frac{1}{(1+\gamma)\frac{da}{dN}} da \tag{15}$$

where da/dN represents the crack propagation rate for long cracks, and γ is the coupling coefficient. The value of γ reflects the influence of the corrosion–fatigue coupling effect on the lifespan. The calculation results of comparative cases with different initial crack value and pit depth can be found in Table 2.

Table 2. Calculation value of coupling coefficient.

Case Information		Case 1	Case 2	Case 3	Case 4	Case 5	Case 6	Case 7	Case 8	Case 9
Single fatigue source expansion	a_p/mm	0.136	0.277	0.167	0.434	0.219	0.337	0.116	-
	a_0/mm	0.003	0.005	0.003	0.008	0.004	0.006	0.002	-
	φ	1.212	1.194	1.241	1.154	1.216	1.176	1.276	-
	γ	0.160	0.049	0.125	0.051	0.013	0.000	0.037	-
Multi-fatigue source expansion	a_p/mm	0.395	0.105	0.177	0.118	0.181	0.155	0.152	0.238
	a_0/mm	0.008	0.004	0.005	0.005	0.006	0.005	0.005	0.006
	φ	1.157	1.226	1.198	1.219	1.197	1.205	1.206	1.183
	γ	0.368	0.247	0.024	0.206	0.097	0.267	0.000	0.428

It should be noted that the γ value in the above equation does not represent the specific influence on a particular crack propagation rate. Instead, it introduces the γ value in the form of the Paris integral equation to comprehensively represent the reduction effect of corrosion fatigue on the calculated lifespan. As shown in Table 2, the γ value exhibits significant variability and does not remain within a certain range. The maximum

value is 0.428, and the minimum value is approximately 0.013, with 0 indicating no effect from corrosion fatigue and symbol of "-" in the table indicating blank. In theory, the γ value should remain constant. However, in practice, it is influenced by crack closure effects (especially for small cracks) and the passivation phenomenon on the steel surface. The corrosive medium may not always affect crack propagation. The γ value shows larger values for multiple fatigue crack growth types compared to a single fatigue source growth. This is believed to be primarily due to the promotion of fatigue sources by the corrosive medium.

4. Corrosion Fatigue Lifespan Assessment of Parallel Wire Cable

A cable lifespan assessment model, which takes into account the corrosion fatigue effect, is proposed based on the series–parallel fiber bundle model. Using the Runyang Suspension Bridge as a case study, the measured stress time history spectrum is employed to conduct parameterized lifespan analysis of the cable. The analysis considered various factors, including traffic loads, initial defects, temperature, and humidity, and their effects on the cable lifespan.

4.1. Cable Life Evaluation Model Considering Corrosion Fatigue Effect

When dealing with the load-bearing capacity of parallel wire cables, the bundle-based series–parallel model is a commonly used method. The main idea is to consider the cable as a parallel combination of equi-length wires with each wire being treated as a structure composed of a certain number of wire units connected in series. Friction units are used between adjacent wires to represent micro-motion wear between wires. For parallel wire cables, especially suspension cable systems, the stress on the wires is primarily uniaxial tension, so the friction effects between the wires can be omitted.

Corrosion in cable systems is mainly manifested as external corrosion and internal corrosion, with the former having a greater impact. When the sheath cracks, the wires come into contact with the external corrosive environment directly. Therefore, the focus in this paper is primarily on the influence of external corrosion on the cable while neglecting the effects of wear between wires. As shown in Figure 10, due to the spatial arrangement of the wires, the influence of the corrosive environment on the corrosion transmission path of individual wires varies within the cable. Therefore, under a specified stress amplitude, each wire will have a different time to fracture. The cable is considered to have failed when the specified wire breakage rate is reached.

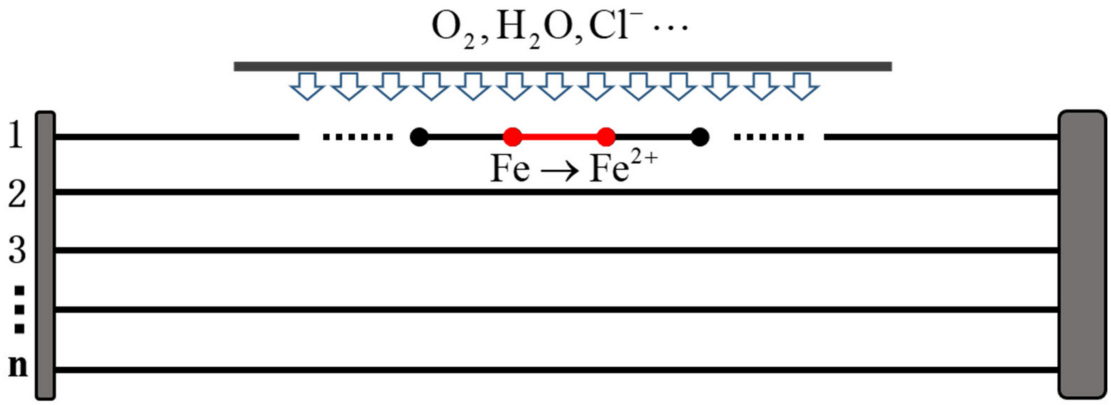


Figure 10. Parallel wire cables whole lifespan calculation model.

The corrosion failure process of a corroded cable system mainly includes the failure of the corrosion protection system and the failure of the wire's load-bearing system. The failure of the corrosion protection system for the wires primarily refers to the corrosion of the coating. The failure of the wire's load-bearing system occurs during the entire stage from the onset of corrosion of the bare wire to its fracture. This includes uniform

corrosion and pitting corrosion of the bare wire. After the occurrence of pitting corrosion, the pits undergo three stages: nucleation, growth, and transformation into cracks. The wire fractures when the crack extends to the critical fracture depth. The parallel wire cables corrosion transfer process is shown in Figure 11.

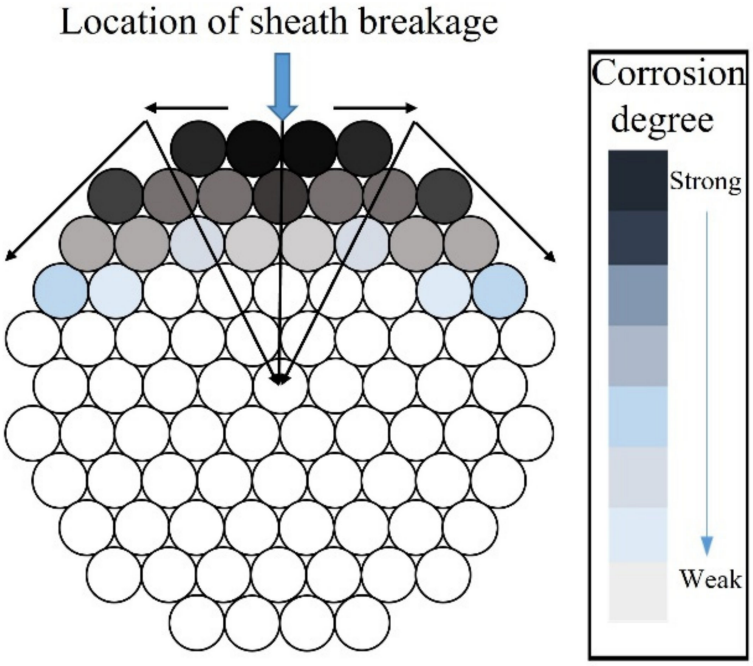


Figure 11. Parallel wire cables corrosion transfer schematic.

After simplifying the parallel wire cables to a series–parallel model, stress redistribution occurs in the parallel wire cables when breakage occurs in a single wire. The fatigue stress after wire breakage is calculated using the following equation:

$$\sigma_{a,i} = \frac{m}{m-i}\sigma_a \tag{16}$$

where m represents the total number of wires in the cable system. i represents the total number of wire breaks after experiencing a certain fatigue load. σ_a is the stress amplitude in the initial state. $\sigma_{a,i}$ is the fatigue stress amplitude after wire breakage.

In the study conducted by Xu [43], the parallel wire ropes from the Shimen Bridge in Chongqing, with different levels of corrosion and corroded cross-sectional distribution, were investigated. They established a statistical corrosion distribution model for corroded wires. To describe the transmission path of corrosive medium within the rope, the model is adopted. The corrosion rate (R) is used to evaluate the transmission process:

$$R = \frac{d_o - d_{\min}}{d_o - d_{\min,0}} \tag{17}$$

where d_0 represents the nominal diameter of the wire, $d_{\min}$ represents the minimum diameter of the remaining wires at other positions on the cross-section, and $d_{\min,0}$ represents the minimum diameter of the reference wire. The expected value of R in the radial direction is $E(R_i) = 0.844^i$, and in the circumferential direction, it is $E(R_i) = 0.868^i$.

After coating corrosion failure, the corrosion products still provide some corrosion protection to the bare wire, and there is a certain incubation period for the initiation of pitting pits after uniform corrosion of the bare wire begins. From a conservative perspective, in the lifespan assessment, it is assumed that the wire enters corrosion of the bare wire,

and pitting pit growth starts immediately after the protective coating fails. The growth of pitting pits is determined based on the deformation of the pitting factor in Equation (18).

$$a_p(t) = \phi_{\max} a_{uc}(t) \tag{18}$$

where $a_p(t)$ represents the maximum pitting depth as a function of time and $a_{uc}(t)$ represents the uniform corrosion depth as a function of time. The pitting factor $\varphi_{\max}$ is used to evaluate the probability distribution relationship of the maximum pitting depth over time.

The Gumbel distribution model for the pitting factor of cable high-tensile steel wires was developed by Li et al. [44] based on the chunked sample extreme value model as shown in Equation (19):

$$F_{\phi_{\max}}(x) = \exp\left(-\exp\left(-\frac{(x-\beta_\kappa)}{\alpha_\kappa}\right)\right) \tag{19a}$$

with coefficients given by

$$\alpha_\kappa = 0.954, \beta_\kappa = 0.905\ln(\frac{A_\kappa}{A_0}) + 4.078 \tag{19b}$$

$$A_\kappa = \pi D L_\kappa, \kappa \geq 3 \tag{19c}$$

where A_0 is the surface area of the steel wire with a length of 21 mm and a diameter of 7 mm, α_κ and β_κ denote the range scale and positional parameters of the surface area A_κ, A_κ is the chunking area and L_κ is the chunking length. When the diameter is 7 mm, A_0 = 329.7 mm^2, α_κ = 0.954, β_κ = 4.078. The series of steel wires used had a diameter of 5 mm, the bare steel quality is the same as that of the literature [44], and the chunking method is used to analyze the probability of corrosion pits according to the surface area of the chunks so that the above model can still be applied.

During the growth process of pitting pits, the pits are simplified into hemispherical shapes, and the transformation criterion is used as a criterion for converting pitting pits into cracks. The transformation criteria are given by the following:

$$(\Delta K)_{pit} \geq \Delta K_{th} \tag{20}$$

$$\frac{da_p}{dt} \leq \frac{da}{dN} \tag{21}$$

$$\Delta K = \frac{1.12 K_t \Delta\sigma\sqrt{\pi a}}{\Phi}\left[\sin^2\theta + (0.5c_p/a_p)^2\cos^2\theta\right]^{1/4} \tag{22}$$

$$\Phi = \int_0^{\pi/2}\left[\sin^2\theta + (0.5c_p/a_p)^2\cos^2\theta\right]^{1/2} d\theta \tag{23}$$

where K_t is the stress concentration coefficient, $\Delta\sigma$ is the stress amplitude, φ is determined to be $\pi/2$, c is half the width of the pit, and a is the pit depth.

Based on the transformation criterion, the corrosion fatigue lifespan N_{CF} can be divided into two stages: crack initiation lifespan N_n (i.e., the lifespan from corrosion pit growth to crack transformation) and crack propagation lifespan N_p.

Equation (24) is used to consider the effect of corrosion–fatigue coupling effect on crack propagation lifespan N_p.

$$\left(\frac{da}{dN}\right)_{CF} = C_{cor}(N)\left(\frac{da}{dN}\right)_F \tag{24}$$

$C_{cor}(N)$ is the correction factor of the corrosion fatigue crack growth rate, which is related to the material, environment and load condition. It should be noted that a large

number of tests are needed to determine this parameter. At present, there is no correction parameter suitable for the corrosion fatigue crack growth rate of high-strength steel wire.

The stress intensity factor (K_{IC}) reaching the fracture toughness value ($\sigma_{\max}$) is considered as the judgment standard for steel wire fracture failure.

$$K_{\max} = Y\sigma_{\max}\sqrt{\pi a_c} \leq K_{IC} \tag{25}$$

$$K_{IC} = 104.5 - 2.1315\eta \tag{26}$$

$$\eta = 1 - (1 - \frac{2a_{uc,Fe}}{D_0})^2 \tag{27}$$

where is the mass loss rate and D_0 is the diameter of the bare steel wire.

4.2. Measured Stress of Bridge Cable

The Runyang Suspension Bridge consists of several sections including the northern approach, the northern bank bridge, the Shiyezhou interchange viaduct, the southern bank bridge, the southern approach, and the extension section. The bridge is located downstream of the Yangtze River, which is subject to high temperatures and humidity throughout the year. Therefore, evaluating its corrosion fatigue performance is of great significance. In this study, the case study refers to the southern bank bridge, which is a single-hole double-cable steel box-girder bridge. The total span of the bridge is 470 + 1490 + 470 m (see Figure 12). The box girders are fabricated by full welding with a streamlined and flat shape, the cross-section has a height of 3 m and a width of 36.3 m. The cable system consists of two main cables and eighty-eighty pairs of hangers. The upper end of the hanger is connected to the main cable via a cable belt, while the lower end is connected to the box girder through an ear plate. In the mid-span, a pair of rigid central clamps is applied to connect the girder to the main cables. The hangers are composed of parallel steel wire ropes, consisting of 109 galvanized high-strength parallel steel wires. The steel wire has a diameter of 5 mm, and the ultimate strength required is not less than 1670 MPa.

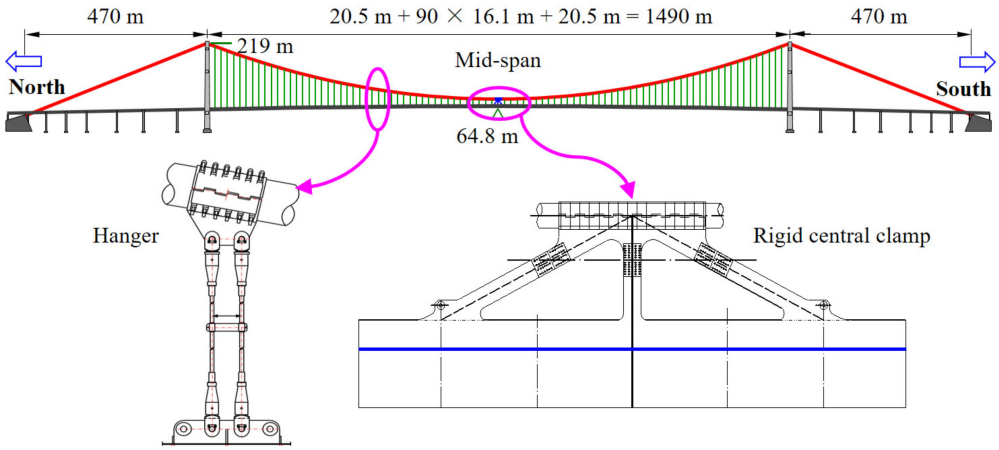


Figure 12. Runyang Suspension Bridge Sketch (Unit: mm).

The suspension cables on each side of the main girders are numbered from north (Yangzhou) to south (Zhenjiang) as No. 1–45, No. 46, and No. 47–91. The No. 46 cable is the central buckle. The spacing between the cables along the bridge is 16.1 m. The suspension cables are made up of 109 galvanized high-strength steel wires with a diameter of 5 mm. The steel wire is required to have a strength of no less than 1670 MPa. To obtain the stress–time history of the suspension cables, displacement sensors were used to measure

the axial deformations of cables. Figure 13 shows the field diagram of the measuring of No. 46 cable. The data acquisition frequency was set to 200 Hz.



Figure 13. Field diagram of cable stress measurement.

The axial stress $\Delta\sigma$ is calculated using the following equation.

$$\Delta\sigma = \frac{\Delta l}{l} E \tag{28}$$

where Δl is the axial deformation of the cable, l is the length of the cable and E is the Young's modulus. Figure 14 presents the processed stress time spectrum, where the extraction time is selected as 500 s.

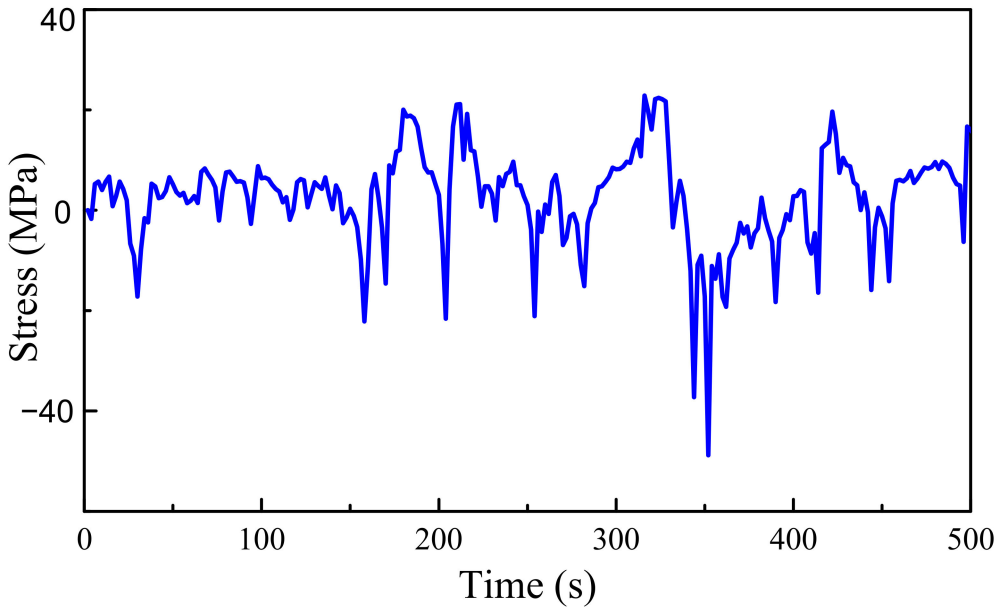


Figure 14. Typical stress time spectrum of cable.

4.3. Load Effect on Corrosion Fatigue Lifespan

The load effect is a crucial factor for the fatigue lifespan of a structure, especially considering the joint effects of corrosion. To measure the effects of corrosion-induced degradation on the bridge load response, Sangiorgio [45] proposed fault trees based on the experience of technicians and numerical simulations of different failure scenarios and successfully applied them to a historic steel truss bridge. Bertolesi [46] conducted a dual experimental and analytical study on the fatigue performance of the Quisi and Ferrandet Bridges and investigated the load effect on the corrosion fatigue lifespan. Based on the inspiration of the above research, this study predicts the corrosion fatigue lifespan of the Runyang Suspension Bridge by calculating the response of the actual active load.

The rainfall counting method is used to process the stress time spectrum, and the equivalent stress amplitude [47] is introduced to calculate the lifespan. The equivalent force amplitude and the number of cycles can be expressed as follows:

$$\sigma_{eq} = \left(\frac{\sum \sigma_{eq} n_i}{\sum n_i} \right)^{\frac{1}{m}} \tag{29}$$

$$N_{eq} = \sum n_i \tag{30}$$

$$f_{eq} = \frac{t_{eq}}{N_{eq}} \tag{31}$$

where σ_i represents the stress amplitude for the ith type, n_i represents the number of cycles, and m represents the slope of the S-N curve, which is assumed to be 3. t_{eq} represents the time duration for that stress amplitude. Calculations yield an equivalent stress amplitude of 23.65 MPa and 70 cycles for the Runyang Suspension Bridge during the specified time period. For the calculation, data with stress amplitudes below 1 MPa are excluded.

The theoretical model proposed in Section 4.1 is adopted. After the coating is completely corroded, the uniform corrosion depth of the bare steel wire is calculated. Assuming the uniform corrosion depth at the current time t_i is $a_{uc,i}$, the uniform corrosion depth can be represented as follows:

$$a_{uc,i} = 1.79011 \cdot [\tau(t_i - t_0)]^{0.62044} \tag{32}$$

Equation (32) represents the uniform corrosion depth of the most severely corroded steel wire inside the sheathing. In the equation, t represents the total time the steel wire has experienced, t_0 represents the time for the coating to be depleted, and τ represents the conversion coefficient between the actual environment and the experimental environment.

Equation (33) is used to investigate the uniform corrosion degree of the remaining cable wires:

$$a_{uc,j} = R_j a_{uc,i} \tag{33}$$

where R_j represents the corrosion ratio of the jth wire.

Assuming that pitting corrosion starts to occur after the coating is completely corroded, the calculation method for the corrosion depth is as follows: sampling is performed for the pit factor $\varphi_{\max}$. When the calculation time reaches t_i, the maximum pit depth calculated is $a_p(t_i)$. When the calculation time reaches t_{i+1}, the maximum pit depth calculated is $a_p(t_{i+1})$. The calculation formula is as follows:

$$a_p(t_{i+1}) = a_p(t_i) + \phi_{\max,i+1}[a_{uc}(t_{i+1}) - a_{uc}(t_i)] \tag{34}$$

The corrosion rate is calculated using the growth rate of pitting pits.

$$v_p = \frac{a_p(t_{i+1}) - a_p(t_i)}{t_{i+1} - t_i} = \phi_{\max,i} \frac{a_{uc}(t_{i+1}) - a_{uc}(t_i)}{t_{i+1} - t_i} \tag{35}$$

When using the aforementioned method for calculation, the influence of the corrosion–fatigue coupling effect on crack propagation is not considered. C_{cor} (corrosion factor) is set as 1 for both conditions. The calculation time interval ($t_{i+1} - t_i$) is set as 1 month. Additionally, considering that the nighttime traffic volume is negligible, the contribution of traffic loads to the fatigue damage of the steel wire can be ignored. Therefore, when calculating the equivalent stress amplitude using the stress spectrum conversion method mentioned above, only the daytime effect is considered. Hence, the time interval for each calculation ($T_{i+1} - T_i$) is set as 15 days.

Currently, the live load on the service cables of bridges is approximately 5% to 12% of the total load [48]. Assuming a constant load of 500 MPa for the cable, the stress fluctuation caused by the live load on the cable wire is estimated to be around 26 to 68 MPa. With the transformation of urban industries, the increase in heavy vehicle traffic will significantly increase the stress fluctuation on the cable wires. In order to compare the effects of different load conditions on the corrosion fatigue lifespan, a baseline stress level of 23.65 MPa is considered. Further analysis is conducted to compare the fatigue lifespan under equivalent stress amplitudes of 40, 50, 60, and 70 MPa. All load conditions are exposed to the same corrosion environment, where the complete depletion of the 30 μm thick galvanized coating in that environment takes approximately 4.9 years. The conversion coefficient τ for this environment is assumed to be 0.1985.

Figure 15 shows the variation of defect depth in the bridge wires under different stress amplitudes. Due to the relatively small stress amplitude caused by the load on the suspension ropes, it takes a long time for pitting corrosion to transition into cracks. When the equivalent stress amplitude is 23.65 MPa, the pitting depth needs to reach 1.179 mm before transitioning into a crack. However, due to the large depth, the converted crack will quickly propagate and fracture, with the crack propagation time estimated to be around 1–2 years. As the stress amplitude gradually increases, the transition depth decreases. When the stress amplitude reaches 70 MPa, the transition time falls within 100 years.

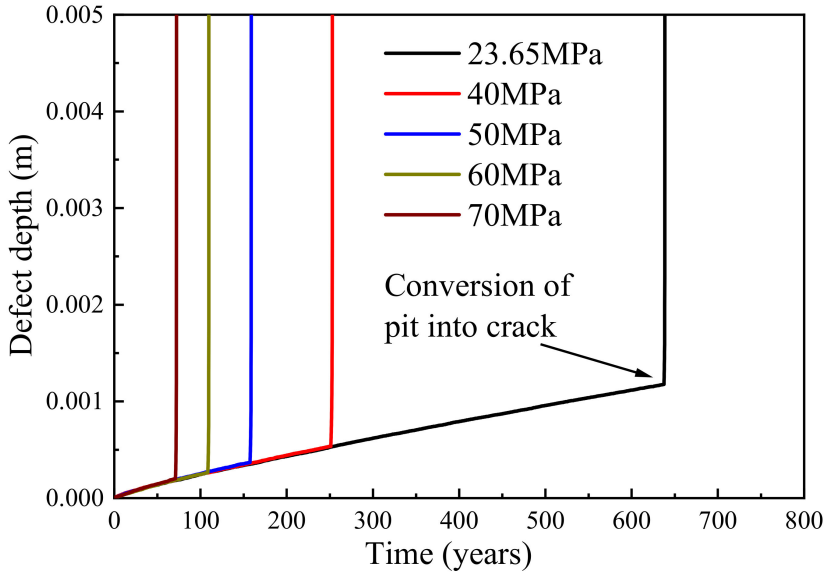


Figure 15. Evolution of defect depths under different stress amplitudes.

With the increase in stress amplitude, the fatigue lifespan gradually decreases. The fatigue lifespan corresponding to 23.85 MPa is approximately 639 years, while it decreases to 73 years when the stress amplitude increases to 70 MPa. The calculation results indicate that within the 100-year reference period for bridge design, the wire will not experience corrosion fatigue fracture. However, this does not necessarily imply that the wire can still safely serve in practical conditions. The initiation mechanism of corrosion fatigue cracks includes four categories, and pitting-induced cracks are just one of them. Additionally,

multiple pits may grow together on this cross-section. Within the design reference period, plastic fracture caused by significant cross-section loss is prone to occur.

Furthermore, considering the evolution of defect size within the internal strands of the cable when the equivalent stress amplitude is 70 MPa, the time for progressive fracture of each strand in a 109-strand wire cable under the current corrosion environment is calculated and presented in Figure 16. The fracture lives of the 2nd, 4th, 6th, 8th, and 10th strands are estimated to be approximately 76, 93, 96, 107, 118, and 131 years, respectively. As shown in Figure 9, due to the symmetric nature of the corroded wire cross-section, when the 2nd, 4th, 6th, 8th, and 10th strands fracture, the 3rd, 5th, 7th, and 9th strands will also fracture in a relatively short time. According to the Technical Specification for Maintenance of Urban Bridges (CJJ 99-2003) [49], when the cable reaches a 2% fracture rate, it is required to be replaced. For a 109-strand steel cable with an estimated operational lifespan of approximately 93 years, the cable will fail and reach the replacement criteria.

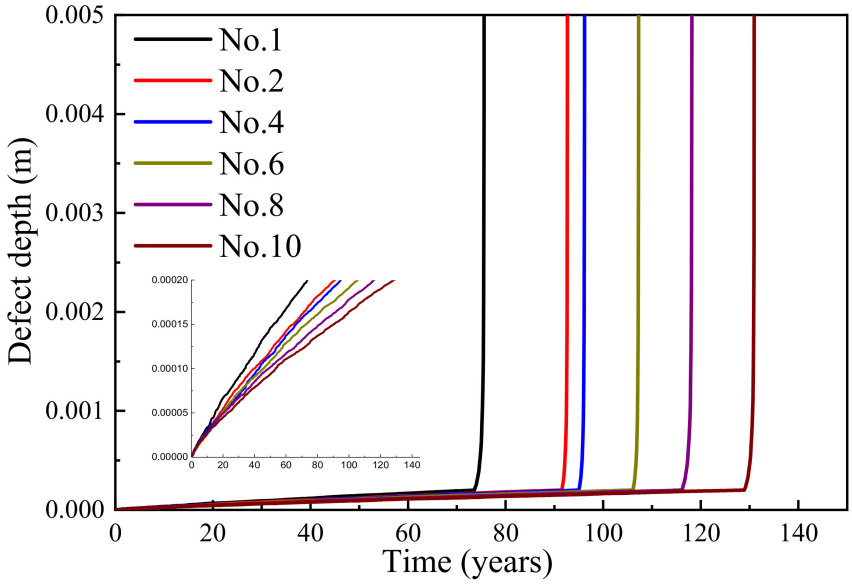


Figure 16. Evolution of the defect depth in each wire of bridge cable.

In reality, the steel wires used in bridge cable strands are made from high-quality high-carbon steel round bars, which undergo isothermal quenching and drawing during the manufacturing process. However, they inevitably have processing defects and residual stresses along with construction scratches that occur during transportation and installation. Under the combined influence of corrosive media and stress, these defects are prone to initiate cracks. In the corrosive fatigue environment, metals often do not exhibit a clear fatigue strength [50]. Steel wires with initial cracks can still experience corrosion fatigue failure albeit over a longer period [51] of time. Therefore, the threshold effect is neglected when considering crack propagation.

When measuring microscopic defects in steel wires with tensile strengths greater than 1800 MPa, Verpoes et al. [51] noted that such initial defects were roughly in the range [2.5 μm, 13 μm]. To facilitate comparing the effects of different defect sizes on the lifespan, these initial defects are treated as equivalent cracks for calculation purposes. Five levels of initial crack depths are selected for comparison: 2.5 μm, 5 μm, 7.5 μm, 10 μm, and 13 μm. The calculations are conducted with an equivalent stress amplitude of 23.65 MPa while keeping the environmental conditions consistent across different operating conditions. The conversion coefficient τ is set to 0.1985, and the fatigue crack growth rate modification factor Ccor is taken as 1.

As shown in Figure 17, the corresponding lifespan for defect sizes of 2.5 μm, 5 μm, 7.5 μm, 10 μm, and 13 μm are 594, 420, 339, 289, and 248 years, respectively, with a decreasing rate of lifespan reduction. Additionally, the crack evolution starts with a very

small size and maintains a relatively long stable period. During this time, the crack depth does not exhibit significant changes, but the pit growth depth noticeably increases. In this stage, due to the slow crack propagation rate, the crack tip tends to degrade into a pit. However, as the pit growth rate gradually decreases, in the later stages of crack growth, excessive stress intensity factors will rapidly lead to fracture propagation.

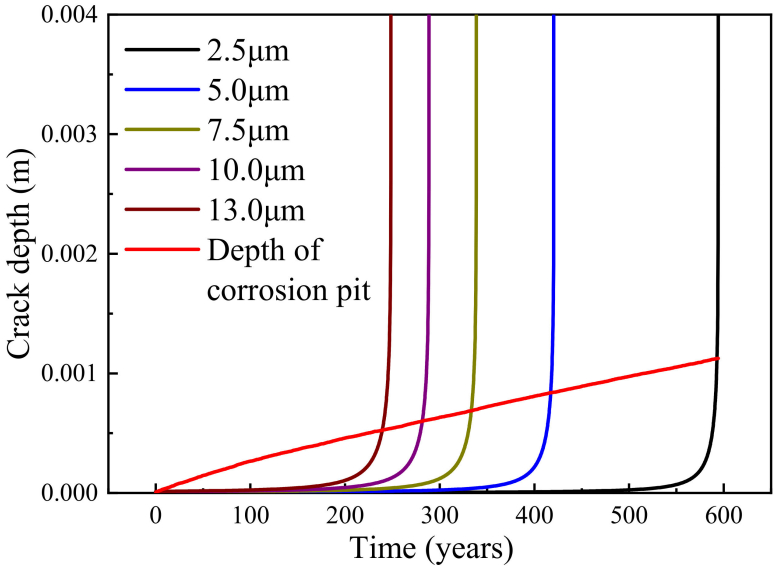


Figure 17. Effect of different initial defect depths on lifespan.

Furthermore, the crack propagation relationships were further compared when the fatigue crack growth rate modification factor C_{cor} was taken as 1, 3, and 5, as shown in Figure 18. The calculations revealed that the lifespan with C_{cor} = 1 is approximately 250 years, which is a value much larger than the design reference period for bridges (100 years). However, when C_{cor} reaches 2, the crack propagation lifespan will be less than 100 years, and when C_{cor} reaches 3, the remaining lifespan is 57 years. While it is not clear how C_{cor} relates to the environment, it at least indicates that under extreme conditions, corrosion fatigue fracture can still occur within the design reference period for bridge cable wires subjected to small stress amplitudes.

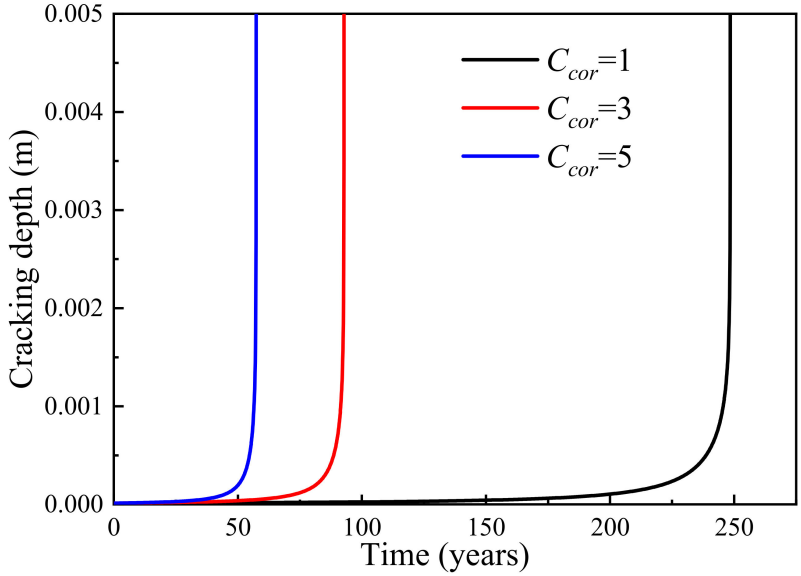


Figure 18. Relationship between C_{cor} and the amount of crack extension.

4.4. Service Environment Effect on Corrosion Fatigue Lifespan

The corrosive environment in Section 4.3 is an industrial environment where a 24 μm-thick pure zinc coating is corroded within 3.9 years. The corrosion rate in this environment is approximately 1.95×10^{-13} m/s. According to the experiments [26], the initial corrosion rate of bare steel wire is about 0.133 times that of zinc, which is approximately 2.59×10^{-14} m/s. This result is much lower than the corrosion rate of uncoated steel wire at the specified temperature and humidity provided in Table 3 [52]. However, the actual environment is much more severe because the Runyang Suspension Bridge is located in the middle and lower reaches of the Yangtze River, where there is a long rainy and foggy season, and it is exposed to high humidity and high-temperature conditions throughout the year. Liao et al. [53] provides statistics on the temperature and humidity annual profile of the Runyang Suspension Bridge, indicating that humidity exceeds 70% for approximately 77.4% of the year. To consider the influence of different environments on corrosion fatigue lifespan, the conversion coefficient (τ) is adjusted to account for the severity of the environment.

$$\tau = \tau_0 \cdot \frac{v_c}{v_{c,0}} \tag{36}$$

where τ_0 represents the conversion coefficient value of the industrial environment that can cause the 24 μm-thick pure zinc coating to corrode completely within 3.9 years with respect to the experimental environment. $v_{c,0}$ corresponds to the corrosion rate of bare steel wire in that industrial environment, and v_c corresponds to the corrosion rate of bare steel wire under different temperature and humidity conditions.

Table 3. Wire corrosion rate values under different combinations of temperature and humidity levels (units: m/s).

Temperature/°C	Humidity Level/%					
	50~60	**70**	**75**	**80**	**85**	**90**
10	7.431×10^{-15}	5.8×10^{-14}	2.48×10^{-13}	3.29×10^{-13}	4.08×10^{-13}	4.25×10^{-13}
20	1.5817×10^{-13}	2.01×10^{-13}	2.28×10^{-13}	3.1×10^{-13}	4.85×10^{-13}	5.39×10^{-13}
30	1.6596×10^{-13}	1.83×10^{-13}	1.86×10^{-13}	2.78×10^{-13}	3.35×10^{-13}	7.32×10^{-13}
40	1.1253×10^{-13}	1.77×10^{-13}	1.89×10^{-13}	5.93×10^{-13}	8.08×10^{-13}	1.43×10^{-12}
50	5.3786×10^{-14}	1.69×10^{-13}	4.15×10^{-13}	9.06×10^{-13}	1.27×10^{-12}	1.8×10^{-12}

Based on the average temperature of 20 °C as a reference, this study further calculated the fatigue lifespan of the steel wires in Runyang Suspension Bridge cable under five humidity environments: 70%, 75%, 80%, 85%, and 90%, with an equivalent stress amplitude of 23.65 MPa. The calculation method involves amplifying the conversion coefficient τ based on the ratio of the corrosion rate provided in Table 3 to 2.59×10^{-14} m/s. As shown in Figure 19, the calculation results indicate that the fatigue lifespan of the steel wires gradually decreases with increasing humidity. The respective lifespan spans are 88, 72, 57, 37, and 34 years. An increase in humidity by 20% results in a reduction of approximately 54 years in lifespan. This demonstrates the significant impact of humidity on the fatigue lifespan.

The corrosion condition of the main cable of a suspension bridge was analyzed by Li et al. [54], and it was found that the exterior of the cable undergoes a cycle of wet and dry conditions during day and night, while the interior and sides are consistently exposed to high humidity, and the bottom is immersed in water. When the protective sheath is cracked, a situation arises where the steel wires are exposed to high humidity or immersed in a water solution for an extended period, resulting in a severe corrosion environment for the wires. Therefore, this study further conducted a comparative analysis of the lifespan at a humidity of 90% under different temperatures ranging from 10 to 50 degrees Celsius. The results are shown in Figure 20. The calculated results demonstrate that in a high-humidity environment, the lifespan gradually decreases with increasing

temperature. When the temperature rises from 10 to 50 degrees Celsius, the lifespans are as follows: 39, 29, 24, 14, and 12 years, respectively. The lifespan decreases from 39 to 12 years as the temperature increases.

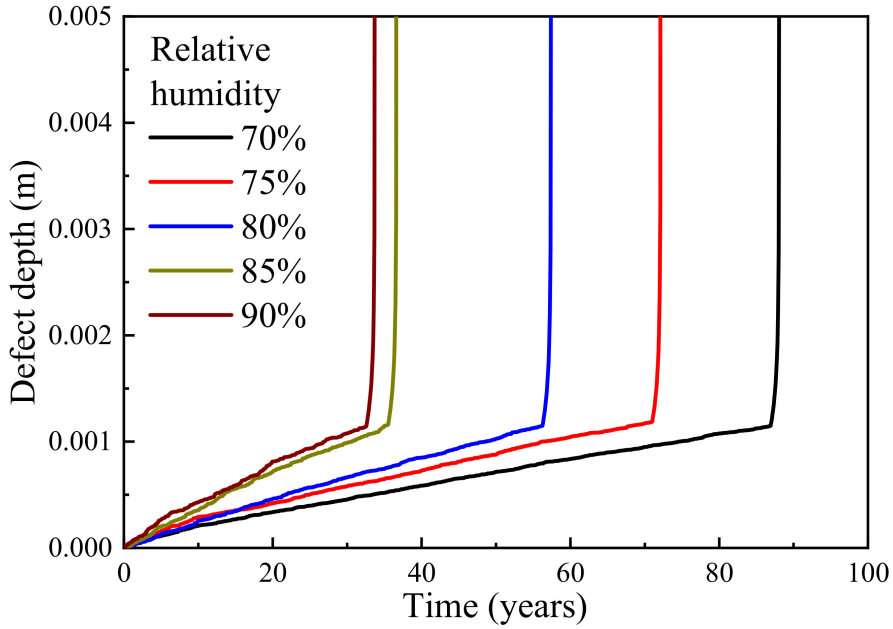


Figure 19. Effect of humidity on wire lifespan.

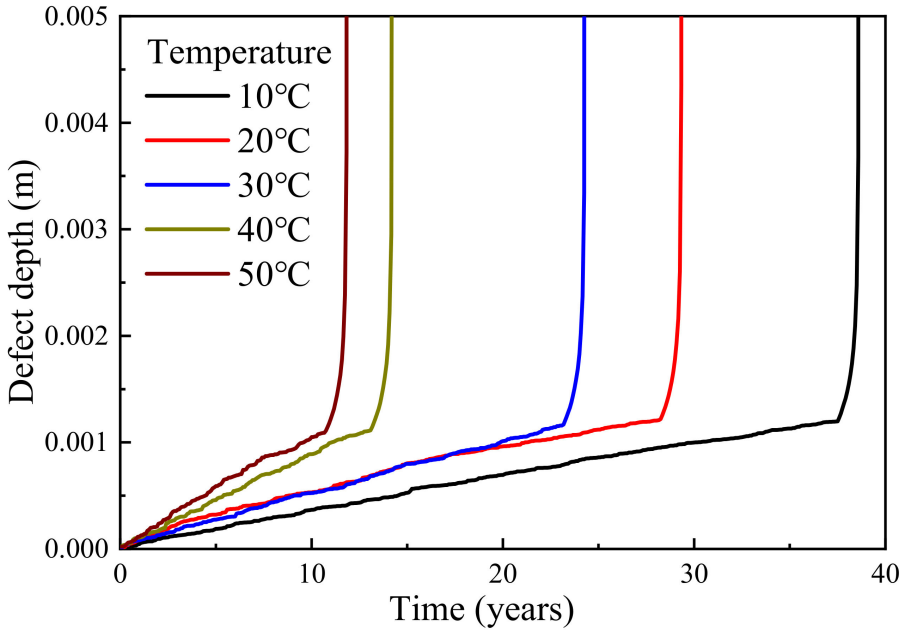


Figure 20. Effect of temperature on wire lifespan.

It can be inferred that temperature and humidity have a more severe impact on the corrosion fatigue lifespan of the steel wires compared to the load. The high-temperature and high-humidity environment accelerates the formation of pitting on the surface of the wires, leading to the initiation of cracks at an earlier stage. To reflect the lifespan of suspension cables in a high-temperature and high-humidity environment, the individual lifespans of the 109 steel wires in the cable were calculated at a temperature of 20 °C, humidity of 90%, and an equivalent stress amplitude of 23.65 MPa. The results are shown in Figure 21. The lifespans of the 1st, 2nd, 4th, 6th, 8th, and 10th wires correspond to 34, 39,

43, 44, 47, and 57 years, respectively. For the entire cable with 109 wires, when the specified failure rate is reached, the service lifespan is approximately 39 years. By comparing with Figure 16, it can be observed that the detrimental effect of the corrosive environment on the corrosion fatigue lifespan is much more significant than that of the load.

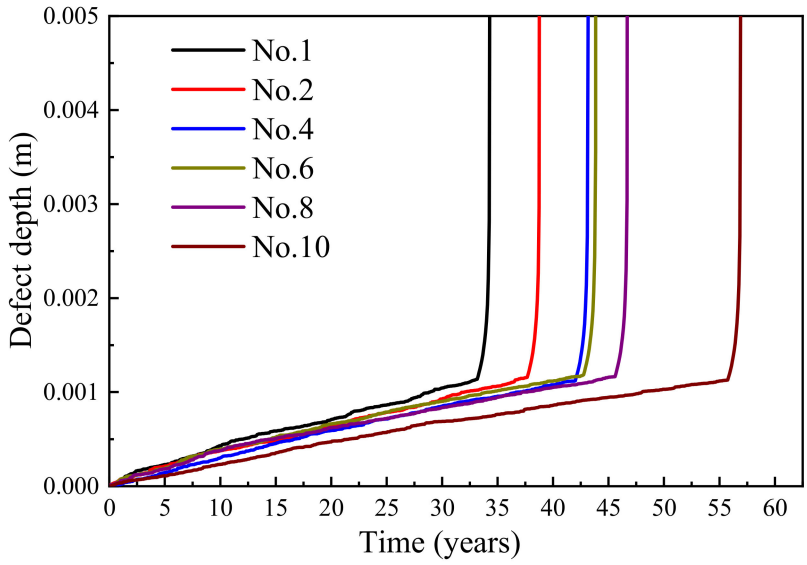


Figure 21. Lifespan of cable wires in severe environment.

5. Conclusions

This study presents a lifespan calculation model based on the EIFS method to analyze the various stages of corrosion wire lifespan. Using this lifespan calculation model, the influence of corrosion and corrosion fatigue coupling on the lifespan of corroded wires is quantitatively discussed. Furthermore, the corrosion fatigue lifespan of the parallel wire suspension cable is investigated based on the series–parallel fiber bundle model. The Runyang Suspension Bridge is used as a case study to evaluate the corrosion fatigue damage evolution of bridge cables during service. Several conclusions can be summarized as follows:

(1) Building upon the EIFS method calculation model, this study further analyzes the influence of corrosion and fatigue load coupling on the corrosion fatigue performance of rusted steel wires. The results indicate that under corrosion fatigue conditions, the initiation of cracks in steel wires is more prone, and their fracture toughness is further reduced. However, this coupling effect does not increase the number of fatigue sources. The factors affecting the number of fatigue sources are primarily the number of pits along the circumference of the steel wire.

(2) Based on the series–parallel fiber bundle model, a corrosion fatigue full lifespan model for parallel wire suspension cables is provided. The parallel wire cables are simplified as independent individual wires connected in parallel. The corrosion propagation model is used to consider the interrelation between each wire, and the conversion criteria are applied to calculate the corrosion fatigue full lifespan of the parallel wire suspension cables.

(3) A case study of the Runyang Suspension Bridge is taken, and the stress time history spectra of short cables near the central clamp are measured. The analysis results of the case study demonstrate that under weak corrosion conditions, the cable wires of the Runyang Suspension Bridge under traffic load will not experience corrosion fatigue fracture during the design reference period. Even under severe traffic loads (calculated based on an equivalent stress amplitude of 70 MPa), the cables can still serve safely. When the steel wire has initial defects, the fracture lifespan under corrosion fatigue conditions depends on the strength of the corrosive medium. The

effect of the medium on crack propagation is evaluated using the C_{cor} value, with a larger C_{cor} value indicating a more severe reduction in lifespan. Even under low stress amplitudes, the steel wires may still experience fracture within the design reference period.

(4) The influence of the environment is considered using conversion factors. The calculation results indicate that the reduction in corrosion fatigue lifespan in a corrosive environment is significantly greater than that due to heavy loads. For a 109-wire suspension cable, the lifespan under severe loads (equivalent stress amplitude of 70 MPa) is approximately 93 years, while in a severe corrosive environment, the lifespan is about 39 years. Therefore, when constructing or maintaining suspension cable facilities, the impact of environmental corrosion should be considered as a primary factor.

Author Contributions: Conceptualization, T.G.; methodology, T.G. and X.Y.; software, Z.L.; validation, X.Y. and S.N.; formal analysis, T.G. and Z.L.; investigation, Z.L and X.Y.; resources, T.G.; data curation, Z.L. and X.Y; writing—original draft preparation, Z.L. and X.Y; writing—review and editing, T.G., S.N. and J.C.; visualization, T.G.; supervision, T.G.; project administration, T.G. and J.C.; funding acquisition, T.G. All authors have read and agreed to the published version of the manuscript.

Funding: This research was funded the Provincial Policy Guidance Program of Jiangsu (grant No. BZ2021011), the Natural Science Foundation of Jiangsu Province (grant No. BK20210257), the Natural Science Foundation of China (grant Nos. 51978156 and 52108272), and the National Key R&D Program of China (grant No. 2022YFB2602700).

Institutional Review Board Statement: Not applicable.

Informed Consent Statement: Not applicable.

Data Availability Statement: All data used are available from the corresponding author upon reasonable request.

Conflicts of Interest: The authors declare no conflict of interest.

References

1. Liu, Z.; Guo, T.; Chai, S. Probabilistic Fatigue Life Prediction of Bridge Cables Based on Multiscaling and Mesoscopic Fracture Mechanics. *Appl. Sci.* **2016**, *6*, 99. [CrossRef]
2. Liu, Z.; Guo, T.; Hebdon, M.H.; Han, W. Measurement and Comparative Study on Movements of Suspenders in Long-Span Suspension Bridges. *J. Bridge Eng.* **2019**, *24*, 04019026. [CrossRef]
3. Lu, N.; Beer, M.; Noori, M.; Liu, Y. Lifetime Deflections of Long-Span Bridges under Dynamic and Growing Traffic Loads. *J. Bridge Eng.* **2017**, *22*, 04017086. [CrossRef]
4. Mayrbaurl, R.M.; Camo, S. Cracking and Fracture of Suspension Bridge Wire. *J. Bridge Eng.* **2001**, *6*, 645–650. [CrossRef]
5. Deng, Y.; Ju, H.; Zhong, G.; Li, A.; Ding, Y. A general data quality evaluation framework for dynamic response monitoring of long-span bridges. *Mech. Syst. Signal Process.* **2023**, *200*, 110514. [CrossRef]
6. Xu, J.; Chen, W. Behavior of wires in parallel wire stayed cable under general corrosion effects. *J. Constr. Steel Res.* **2013**, *85*, 40–47. [CrossRef]
7. Fan, Z.; Xu, X.; Ren, Y.; Chang, W.; Deng, C.; Huang, Q. Fatigue reliability analysis for suspenders of a long-span suspension bridge considering random traffic load and corrosion. *Structures* **2023**, *56*, 104981. [CrossRef]
8. Jiang, C.; Xiong, W.; Cai, C.S.; Zhou, L.; Zhu, Y. Fatigue assessment of fillet weld in steel bridge towers considering corrosion effects. *Eng. Fail. Anal.* **2023**, *143*, 106901. [CrossRef]
9. Liu, Z.; Shi, X.; Guo, T.; Yang, J.; Correia, J. Damage diagnosis and fretting wear performance analysis of short suspenders in cable-supported bridges. *Structures* **2023**, *56*, 104909. [CrossRef]
10. Fan, Z.; Ye, Q.; Xu, X.; Ren, Y.; Huang, Q.; Li, W. Fatigue reliability-based replacement strategy for bridge stay cables: A case study in China. *Structures* **2022**, *39*, 1176–1188. [CrossRef]
11. Ma, Y.; He, Y.; Wang, G.; Wang, L.; Zhang, J.; Lee, D. Corrosion fatigue crack growth prediction of bridge suspender wires using Bayesian gaussian process. *Int. J. Fatigue* **2023**, *168*, 107377. [CrossRef]
12. Liu, X.; Han, W.; Guo, X.; Yuan, Y.; Chen, S. Fatigue lifespan assessment of stay cables by a refined joint probability density model of wind speed and direction. *Eng. Struct.* **2022**, *252*, 113608. [CrossRef]
13. Yuan, Y.; Liu, X.; Pu, G.; Wang, T.; Zheng, D. Temporal and spatial variability of corrosion of high-strength steel wires within a bridge stay cable. *Constr. Build. Mater.* **2021**, *308*, 125108. [CrossRef]

14. Yuan, Y.; Liu, X.; Pu, G.; Wang, T.; Guo, Q. Corrosion features and time-dependent corrosion model of Galfan coating of high strength steel wires. *Constr. Build. Mater.* **2021**, *313*, 125534. [CrossRef]
15. Liu, Z.; Guo, T.; Han, D.; Li, A. Experimental Study on Corrosion-Fretting Fatigue Behavior of Bridge Cable Wires. *J. Bridge Eng.* **2020**, *25*, 04020104. [CrossRef]
16. Godard, H.P. The corrosion behavior of aluminum in natural waters. *Can. J. Chem. Eng.* **1960**, *38*, 167–173. [CrossRef]
17. Ezuber, H.; El-Houd, A.; El-Shawesh, F. A study on the corrosion behavior of aluminum alloys in seawater. *Mater. Des.* **2008**, *29*, 801–805. [CrossRef]
18. Fu, Y.; Yue, S.; Changbo, D.; Jun, L. Determination Method of Reliability Index of Main Cable Life of Suspension Bridge. *J. Disaster Prev. Mitig. Eng.* **2020**, *40*, 358–364. [CrossRef]
19. Kim, Y.H.; Fine, M.E. Fatigue crack initiation and strain-controlled fatigue of some high strength low alloy steels. *Metall. Trans. A* **1982**, *13*, 59–72. [CrossRef]
20. Zhang, X.; Zhu, H.; Liu, Y.; Li, D. A Fatigue Life Assessment Method for Arch Bridge Suspension Rods Based on Monitoring Data and Its Application. *J. Disaster Prev. Mitig. Eng.* **2010**, *30*, 314–317. [CrossRef]
21. Donahue, J.R.; Lass, A.B.; Burns, J.T. The interaction of corrosion fatigue and stress-corrosion cracking in a precipitation-hardened martensitic stainless steel. *npj Mater. Degrad.* **2017**, *1*, 11. [CrossRef]
22. Olive, J.M.; Cwiek, J.; Desjardins, D. Quantification of the hydrogen produced during corrosion fatigue crack propagation. *Corros. Sci.* **1999**, *41*, 1067–1078. [CrossRef]
23. Shipilov, S.A. Location of the fracture process zone for hydrogen-induced corrosion fatigue crack propagation. *Scr. Mater.* **2002**, *47*, 301–305. [CrossRef]
24. Llorca, J.; Sanchez-Galvez, V. Fatigue threshold determination in high strength cold drawn eutectoid steel wires. *Eng. Fract. Mech.* **1987**, *26*, 869–882. [CrossRef]
25. Li, H.; Lan, C.M.; Ju, Y.; Li, D.S. Experimental and Numerical Study of the Fatigue Properties of Corroded Parallel Wire Cables. *J. Bridge Eng.* **2012**, *17*, 211–220. [CrossRef]
26. Liu, Z.; Guo, T.; Yu, X.; Huang, X.; Correia, J. Corrosion fatigue and electrochemical behaviour of steel wires used in bridge cables. *Fatigue Fract. Eng. Mater. Struct.* **2021**, *44*, 63–73. [CrossRef]
27. Liu, Y.; Mahadevan, S. Probabilistic fatigue life prediction using an equivalent initial flaw size distribution. *Int. J. Fatigue* **2009**, *31*, 476–487. [CrossRef]
28. FAWAZ, S.A. Equivalent initial flaw size testing and analysis of transport aircraft skin splices. *Fatigue Fract. Eng. Mater. Struct.* **2003**, *26*, 279–290. [CrossRef]
29. Sankararaman, S.; Ling, Y.; Shantz, C.; Mahadevan, S. Inference of equivalent initial flaw size under multiple sources of uncertainty. *Int. J. Fatigue* **2011**, *33*, 75–89. [CrossRef]
30. Merati, A.; Eastaugh, G. Determination of fatigue related discontinuity state of 7000 series of aerospace aluminum alloys. *Eng. Fail. Anal.* **2007**, *14*, 673–685. [CrossRef]
31. Krasnowski, B.R.; Rotenberger, K.M.; Spence, W.W. Damage tolerance method for helicopter dynamic components. *J. Am. Helicopter Soc.* **1991**, *36*, 52–60. [CrossRef]
32. Chen, J.; Diao, B.; He, J.; Pang, S.; Guan, X. Equivalent surface defect model for fatigue life prediction of steel reinforcing bars with pitting corrosion. *Int. J. Fatigue* **2018**, *110*, 153–161. [CrossRef]
33. Lankford, J.; Hudak, S.J. Relevance of the small crack problem to lifetime prediction in gas turbines. *Int. J. Fatigue* **1987**, *9*, 87–93. [CrossRef]
34. Xue, Y.; Horstemeyer, M.F.; McDowell, D.L.; El Kadiri, H.; Fan, J. Microstructure-based multistage fatigue modeling of a cast AE44 magnesium alloy. *Int. J. Fatigue* **2007**, *29*, 666–676. [CrossRef]
35. Wang, L.; Daniewicz, S.R.; Horstemeyer, M.F.; Sintay, S.; Rollett, A.D. Three-dimensional finite element analysis using crystal plasticity for a parameter study of microstructurally small fatigue crack growth in a AA7075 aluminum alloy. *Int. J. Fatigue* **2009**, *31*, 651–658. [CrossRef]
36. Xiang, Y.; Lu, Z.; Liu, Y. Crack growth-based fatigue life prediction using an equivalent initial flaw model. *Part I Uniaxial Load. Int. J. Fatigue* **2010**, *32*, 341–349. [CrossRef]
37. Beretta, S.; Boniardi, M. Fatigue strength and surface quality of eutectoid steel wires. *Int. J. Fatigue* **1999**, *21*, 329–335. [CrossRef]
38. Kaynak, C.; Ankara, A.; Baker, T.J. Effects of short cracks on fatigue life calculations. *Int. J. Fatigue* **1996**, *18*, 25–31. [CrossRef]
39. Huang, Y.; Ye, X.; Hu, B.; Chen, L. Equivalent crack size model for pre-corrosion fatigue life prediction of aluminum alloy 7075-T6. *Int. J. Fatigue* **2016**, *88*, 217–226. [CrossRef]
40. Wang, J.; Zhang, Y.; Sun, Q.; Liu, S.; Shi, B.; Lu, H. Giga-fatigue life prediction of FV520B-I with surface roughness. *Mater. Des.* **2016**, *89*, 1028–1034. [CrossRef]
41. Roffey, P. The fracture mechanisms of main cable wires from the forth road suspension. *Eng. Fail. Anal.* **2013**, *31*, 430–441. [CrossRef]
42. Forman, R.G.; Shivakumar, V. *Growth Behavior of Surface Cracks in the Circumferential Plane of Solid and Hollow Cylinders*; American Society for Testing and Materials: Philadelphia, PA, USA, 1986; pp. 59–64.
43. Xu, J. *Mechanism of Damage Evolution and Assessment of Remaining Service Lifespan of Tie Ropes*; School of Civil Engineering, Tongji University: Shanghai, China, 2006.

44. Li, S.; Xu, Y.; Li, H.; Guan, X. Uniform and Pitting Corrosion Modeling for High-Strength Bridge Wires. *J. Bridge Eng.* **2014**, *19*, 04014025. [CrossRef]
45. Sangiorgio, V.; Nettis, A.; Uva, G.; Pellegrino, F.; Varum, H.; Adam, J.M. Analytical fault tree and diagnostic aids for the preservation of historical steel truss bridges. *Eng. Fail. Anal.* **2022**, *133*, 105996. [CrossRef]
46. Bertolesi, E.; Buitrago, M.; Adam, J.M.; Calderón, P.A. Fatigue assessment of steel riveted railway bridges: Full-scale tests and analytical approach. *J. Constr. Steel Res.* **2021**, *182*, 106664. [CrossRef]
47. Song, Y.; Ding, Y. Fatigue monitoring and analysis of orthotropic steel deck considering traffic volume and ambient temperature. *Sci. China Technol. Sci.* **2013**, *56*, 1758–1766. [CrossRef]
48. Xu, J.; Chen, W.; Liu, X. Degradation Mechanism of Inclined Cable and Steel Wire Mechanical Model. *J. Tongji Univ. Nat. Sci. Ed.* **2008**, *36*, 911–915. [CrossRef]
49. *CJJ 99-2003*; Technical Specifications for Maintenance of Urban Bridges. Ministry of Construction of the People's Republic of China: Beijing, China, 2004.
50. Jiang, J.H.; Ma, A.B.; Weng, W.F.; Fu, G.H.; Zhang, Y.F.; Liu, G.G.; Lu, F.M. Corrosion fatigue performance of pre-split steel wires for high strength bridge cables. *Fatigue Fract. Eng. Mater. Struct.* **2009**, *32*, 769–779. [CrossRef]
51. Verpoest, I.; Aernoudt, E.; Deruyttere, A.; De Bondt, M. The fatigue threshold, surface condition and fatigue limit of steel wire. *Int. J. Fatigue* **1985**, *7*, 199–214. [CrossRef]
52. Chen, X.; Tang, M. Corrosion rate spectra of ungalvanized high-tensile steel wires in temperature and humidity environments. *J. Southwest Jiaotong Univ.* **2018**, *53*, 253–259. [CrossRef]
53. Liao, C.; Wei, T.; Wang, Y.; Wang, M. Experimental study on the corrosion rate of cable wires of large-span bridges. *J. Southwest Jiaotong Univ.* **2014**, *49*, 513–518. [CrossRef]
54. Li, R.; Miao, C.; Wei, T. Experimental study on corrosion behaviour of galvanized steel wires under stress. *Corros. Eng. Sci. Technol.* **2020**, *55*, 622–633. [CrossRef]

Disclaimer/Publisher's Note: The statements, opinions and data contained in all publications are solely those of the individual author(s) and contributor(s) and not of MDPI and/or the editor(s). MDPI and/or the editor(s) disclaim responsibility for any injury to people or property resulting from any ideas, methods, instructions or products referred to in the content.